EXPERIMENTAL CHARACTERIZATION OF A NOVEL INTEGRATED FLOW CONTROL METHOD

A Thesis
Submitted to the Graduate Faculty
of the
North Dakota State University
of Agriculture and Applied Science

By

Muhammad Niamul Baqui

In Partial Fulfillment of the Requirements
for the Degree of
MASTER OF SCIENCE

Major Department:
Mechanical Engineering

November 2010

Fargo, North Dakota

North Dakota State University
Graduate School

Title

Characterization and Application

Of an Integrated Flow Control Method

By

Muhammad Baqui

The Supervisory Committee certifies that this ***disquisition*** complies with North Dakota State University's regulations and meets the accepted standards for the degree of

MASTER OF SCIENCE

ABSTRACT

Baqui, Muhammad Niamul, M.S., Department of Mechanical Engineering, College of Engineering and Architecture, North Dakota State University, November 2010. Experimental Characterization of a Novel Integrated Flow Control Method. Major Professor: Dr. Zakaria Mahmud.

Flow control methods can be used in many areas of aerodynamics such as separation control, wind turbines, landing gears and micro satellites. Flow separation in the boundary layer is one of the fundamental problems of aerodynamics. Separated flow in the airfoil boundary layer causes the aircraft to stall. Blowing and Dielectric Barrier Discharge (DBD) Plasma Actuator based techniques have proven successful in limited applications of separation control. However, Blowing techniques require high pressure source and Plasma Actuators are only successful in low speed application. The current research incorporated experimental techniques in characterizing a novel integrated flow control method by combining blowing flow control with Dielectric Barrier Discharge (DBD) Plasma Actuator based flow control. Integrated control would be applicable in wider flow domain than individual plasma or blowing. Initially, characterization experiments were performed as a proof of concept for the integrated control and then, the integrated control was applied in airfoil separation control. Characterization experiments were performed with a vertically fired cylindrical jet having plasma actuator around the jet periphery. The cylindrical jet was used to simulate blowing. The results obtained from characterization experiments indicated 63% reduction in blowing ratio due to plasma addition. The integrated control was placed on NACA 0025 airfoil with blow opening at 25% x/C and plasma actuator at 25.5% x/C location. Windtunnel tests were performed at freestream velocities of 3 m/s and 4.5 m/s with airfoil angle set at 10 degree. Results indicate 110% increase in airfoil near wall velocity for 3m/s when

integrated control was applied. Separation was experienced in the region when other flow control methods were used.

ACKNOWLEDGEMENTS

I want to thank my adviser Dr. Zakaria Mahmud for his continual support and active guidance in completing this research work. I am also grateful to Mechanical Engineering Department for giving me an opportunity to pursue Masters Degree. I specially want to thank every member of my supervisory committee for their excellent support and fruitful comment.

TABLE OF CONTENTS

LIST OF TABLES

LIST OF FIGURES

NOMENCLATURE

DBD = Dielectric Barrier Discharge

SDBD = Single Dielectric Barrier Discharge

AC = Alternating current

α = Angle of attack

Cd= Coefficient of drag

Cl = Co efficient of lift

x/C = Chordwise distance

PIV = Particle Image Velocimetry

$C\mu$ = Blowing coefficient

NACA = National Advisory Committee for Aeronautics

DAQ = Data Acquisition

kV = Kilo Volts

CHAPTER 1. INTRODUCTION

Flow control can benefit various sectors of aerodynamic application such as separation control over airfoils, wind turbine electricity generation, aircraft performance loss during takeoff-landing, noise control and propulsion in micro satellites. However, separation control over an airfoil has been one of the fundamental problems in aerodynamics where flow control methods can be applied. Flow separation causes the aircraft to stall. Different methods have been developed for flow separation control. Boundary layer blowing and Dielectric Barrier Discharge (DBD) Plasma Actuator has proven successful for separation control in specific applications. However, Blowing techniques require high pressure source and Plasma Actuators are only successful in low speed application. The current research incorporated experimental techniques in characterizing a novel integrated flow control method by combining blowing flow control with Dielectric Barrier Discharge (DBD) Plasma Actuator based flow control. Integrated control would be applicable in wider flow domain than individual plasma or blowing. The work is experimental and can be broadly divided into two parts. In the first part, an investigation is performed to characterize the integrated flow control approach. In second part, the integrated flow control was applied in an airfoil to quantify its effectiveness in flow separation control.

The flow separation occurs when the boundary layer energy falls to zero as it tries to overcome the adverse pressure gradient. In airfoil, the flow becomes separated when it no longer follows surface after an increase of the airfoil angle. Eventually it takes the form of eddies and vortices. The point where the flow is no longer following

the airfoil surface is called the separation point. Flow separation increases the pressure drag and in its most severe form, puts the airfoil into stall condition.

Scientists and Engineers have been working over the years to develop effective and efficient ways to control flow separation. Generally, the measures of flow control can be divided into two broad categories: 1) The Passive Flow Control and 2) The Active Flow Control. The Passive flow control relies on indirect energy addition by incorporating roughness elements on the airfoil surface for flow manipulation. They are effective over a very limited range of operating conditions. They also lack in flexibility of its operation. Some of the most widely used passive flow control techniques are: Dimples, Boundary layer trips, Roughness elements, Ejector nozzles, Surface perturbation, Vortex generators. Passive controls are not suitable for all kinds of flow condition and have limited success in separation control.

The Active control method, on the other hand, requires external energy source for flow manipulation. This method is have been able to produce better results than passive control. Acoustic Excitation, Hydrodynamic Excitation, Mechanical Excitation, Boundary layer suction/blowing and DBD Plasma Actuation are some of the established active control techniques developed so far. Among the active control methods boundary layer momentum addition due to air blow is the most popular and plasma actuator based flow control is the most promising.

The Dielectric Barrier Discharge (DBD) actuator consists of two electrodes. The top electrode is exposed the environment and the bottom is buried under the dielectric material [Figure 1.1]. The classic representation is referred as Single Dielectric Barrier Discharge or SDBD. When the electrodes are supplied with high

enough AC voltage, the air over the bottom electrode gets weakly ionized (less than 1-ppm) [1]. As the AC voltage is applied in the positive half cycle, electrons leave the metal electrode, move and accumulate toward the dielectric. In the negative half cycle, electrons move toward the metal electrode and they are supplied with surface discharges on the dielectric. The timescale of the total process is within a few nanoseconds. The process is also dependent in different parameters such as gas composition, excitation frequency etc. [2]. This ionized gas is referred as the plasma. It appears blue in color and requires dark space for viewing in "naked" eye. In presence of the electric field, the ionized gas creates momentum due to body force influence on the stagnant air. This momentum is the used for active flow control. They can be run in steady and unsteady manner.

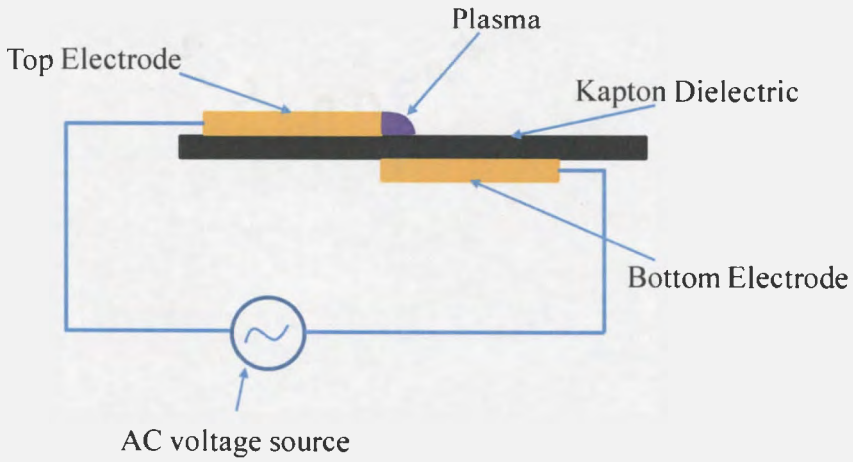

Figure 1.1. Dielectric Barrier Discharge Actuator configuration

One of the major advantages of Plasma Actuators is that it is light weight and low cost. At the same time, it can generate momentum to suppress flow separation. The actuators are tiny and would not require much space in the aircraft. Multiple actuators can be used to generate additional momentum and they can be placed in various

chordwise locations along the airfoil surface. The control over the momentum addition is also easy in this approach. These features of plasma actuators have made it a great choice for separation control and lift enhancement on airfoils. However, the momentum addition by Plasma Actuators is largely dependent on the Dielectric Strength of the barrier material. For low Reynolds number flows, the voltage difference across the barrier would be in the order of several kilo Volts. The barrier should be strong enough to sustain this voltage difference. In high speed flows, higher momentum addition would be needed to have reasonable impact in the boundary layer. Often the dielectric material fails to sustain that voltage difference needed in high speed flows. Plasma actuators also involve too many parameters in its operation and so far no computer or mathematical model have been developed which can address all this parameters at the same time. This possesses a serious challenge in its widespread application of plasma actuator. In reality, flight condition may vary over time so predicting plasma actuator performance is an important part of its successful operation. Since plasma actuators are simple in construction and light weight, they could be very suitable for low pressure application such as micro satellites, where small amount of energy is needed for altitude control. However, plasma actuator requires negative ion content for its thrust generation. In atmospheric condition, the oxygen content in air produces the negative ion for thrust generation but in space, oxygen is not present and plasma would not be able to generate its usual thrust. This limits a highly potential application of plasma actuators as thrusters for microsatellites. These the drawbacks that plasma based flow control are currently facing.

Boundary layer momentum addition by air blow is the most widely used Flow Control technique. In blowing methods, additional momentum is added in the boundary layer in the form ρU^2. The momentum can be added tangentially or at an angle [Figure 1.2]. In most of the cases tangential application produce better results. However, there are special cases when angle blowing performed better than tangential blowing. Blowing can also be done in steady and unsteady manner. In blowing the energy addition can be varied by changing the amount of air injection. The separation on an airfoil changes due to freestream condition change. In blowing methods, the energy addition in the boundary layer can be changed by changing the air injection rate. Depending on the requirement, it can be increased or decreased. This is the reason why blowing have been so successful in controlling flow separation in incompressible and compressible flows. Blowing has been a very popular choice for separation control.

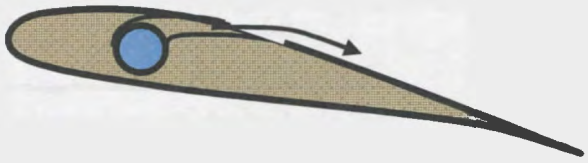

Figure 1.2. Air blow in the boundary layer

Although the air injection can be varied in blowing, the air injection location or the blowing slot will be fixed for each aircraft. The aircrafts fly in different freestream conditions. Separation intensity changes due to freestream influence and airfoil angle change. For blowing, we have a fixed blow opening and that results in inefficient use of blowing energy. In momentum addition by air blow, a high pressure source is required. In most of the cases compressors are used for obtaining this high pressure. Compressors

incorporate additional cost and raise safety concern in its applications. Aircrafts are already equipped with compressors in it but routing that compressed gas posses additional design challenge. Blowing techniques become unfeasible in space for altitude control of micro satellites, since these devices have only a limited storage of compressed cold gas. Blowing techniques are also hard to incorporate in other aerodynamic devices such as wind turbines and landing gears.

Motivation of current research: Both plasma actuator and boundary layer blowing has been successful in flow separation control. Blowing is successful in compressible and incompressible flow regime and is a proven technique of flow separation control. However, blowing techniques are expensive, inefficient and for a particular airfoil their geometric location is fixed. They also raise additional safety measures in their application. Plasma actuators are successful only in low speed flows mostly up to 40 m/s. They have too many parameters involved and at the same time, they do not have a functional computer or mathematical model which can consider all these parameters at the same time. They also rely on negative ion content of air for generating thrust. If DBD plasma actuators are combined with blowing flow control then it would result in a versatile flow control method which is have added benefits of the both control methods.

The integrated plasma with blowing would eliminate the necessity of high pressure source on board and that will result in a cost effective and efficient flow control method. Multiple plasma actuators can be used in different locations of the airfoil for greater momentum addition. Since high pressure sources will be eliminated it will not have safety concerns. At the same time will have additional control since

plasma and blowing techniques can be operated individually if one of them fails to operate in cruise. The integrated control can also benefit the micro satellites in low pressure since blowing could provide the required air or negative ion content for plasma to generate thrust. The current research aims to perform a detailed investigation on the development and application of an integrated flow control approach. The rest of the document is organized as follows: Chapter 2 explores the current state of plasma and blowing flow control research. Chapter 3 presents the experimental setup and procedure. In Chapter 4, results and discussions will be presented. Finally in Chapter 5, conclusions and future development works would be proposed.

CHAPTER 2. BACKGROUND

In this section, a survey has been performed for different research work done earlier to explore the current state of Plasma based and Blowing flow control research. In the later portion of the chapter, the motivation and objectives of current work will be stated.

2.1. Plasma Flow Control

It has been observed that both physical parameters and electrical properties contribute to the performance of plasma actuator. A combination of all these parameters and properties can generate plasma which will be effective for a certain flow condition. For plasma performance, induced velocity (m/s, cm/s) was seen to be the control parameter. Since plasma actuator involves so many parameters, a mathematical model can play a significant role in optimizing its performance. However, the model produces so far lacks to address all these parameters at the same time.

The dielectric material, the gap between top and bottom electrode are the physical parameters that govern the plasma performance (Roth and Dai[3], . Pons et. al [4], Forte et. al [5], Van Dyken et. al [6]. Post et. al [7]). Alumina, Kapton, Quartz and Teflon are the dielectric materials used in plasma actuators. Among these materials, Kapton is most widely used in flow control devices because of its flexibility

The electrical properties also contribute to a great extent in the actuator performance. The AC signal shape, the magnitude of voltage and frequency are the major properties for plasma actuator output (Roth and Dai[3], Post et. al [7], Ramakumar et. al [8], Enloe et. al [9], . Porter et. al [10], McLauglin et. al [11], Roth

Sherman et. al [12], Jacob[13] et. al, Porter [14]et. al, Rivir [15] et. Al, Leonov et. al [16]) . Among the AC voltage signals, Sine wave has been the most widely used in plasma actuators. Plasma actuator output is largely governed by the magnitude of AC input voltage. With an increase in voltage, a corresponding increase in induced velocity is observed. Roth Dai [3] observed reduction in induced velocity when plasma voltage increased from 5kV to 10kV. However, in the study of Balcer [17] et.al, they found when plasma power was increased from 20W to 40 W; plasma induced high velocity in the boundary layer. This finding clearly indicates the influence of different parameters of plasma actuator. A functional simulation model would have been able to better predict its performance.

Bejawada [18] et. al performed a detailed parametric study to explore the different parameters that affect the DBD actuators performance. In their study they investigated the affects of Dielectric material, Electrode gap, Actuator voltage, Signal frequency and Power waveform shape on a flat plate DBD actuator performance. They tested the influence of Alumina and Kapton dielectric; 1mm overlap, no overlap, 1 mm gap between actuators; Voltage variation from 1.45 to 4.2 KVrms; Signal frequency from 5 -15 kHz and Sine wave in DBD actuator performance. Among various results for Kapton dielectric, they found the maximum velocity induced by plasma actuator was 1780 mm/sec. They have also explored that in all cases the increase in actuator voltage has resulted in an increase on flow velocity. Although for their case the voltage of 4.3 kVrms and frequency of 12 kHz for kapton dielectric gave the best performance, they also have experienced an increase in flow velocity for lower voltage and frequency combinations. Figure 2.1 presents the voltage, velocity and frequency relations for

Kapton dielectric with no gap between the electrodes that Bejawada [18] et. al found in their analysis.

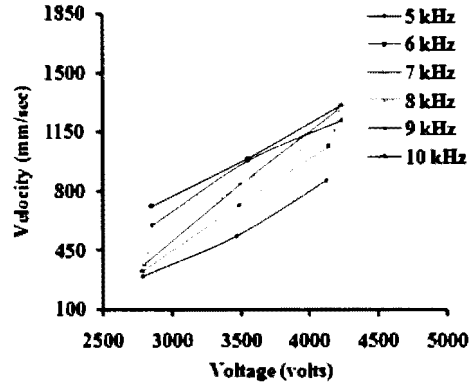

Figure 2.1. Velocity vs. voltage plot for Kapton [18]

Plasma actuators have been applied successfully as a separation control device in various applications. Jacob[13] et. al performed investigation in boundary layer flow control with AC plasma actuator. With 7 inches long single electrodes mounted on acrylic substrate for wind tunnel flows varying over Re 30k to 50k, they found velocity increment in near wall region with plasma integration. For their flow conditions, they also found the influence of duty cycles in the plasma induced flow. Balcer et. al[17] used plasma actuators for separation control on a flat surface similar to the suction surface of a Pack-B turbine blade, and the exposed electrode was oriented sixty degrees to freestream direction. They observed an increase in near-wall velocities when plasma actuator was turned on. Post, Corke[19] performed separation control experiments in NACA 0015 airfoil at high angle of attack in stationary and periodic oscillating conditions. The plasma actuator was operated in both steady and unsteady operating conditions. The chord and span of the airfoil was 12.7 cm and 25.4 cm respectively. The plasma actuator was located right at the leading edge of airfoil i.e. x/c=0. In this case

the actuator was placed before the separation point. For stationary airfoil at Re_c of 158k, a single plasma actuator at leading edge that operated in a steady manner was able to reattach the flow for angles of attack up to 22 degrees which was 8 degrees past the normal stall angle. Under these conditions, the lift-to-drag ratio increased by as much as 300 percent.

Apart from being a separation control device, plasma actuator was also used successfully as flaps and slats in airfoils. Corke, He[20] et. al investigated the performance of plasma actuator as flaps and slats into NACA 0015 airfoil. The actuators were located at leading and trailing edges of the airfoil i.e. x/c=0 and x/c=0.9. Flow control tests were done at Reynolds number of 217k and 307k. The airfoil dimensions were 12.7 cm chord and 30.48 cm in span. At the leading edge, the actuator was operated in both a steady and unsteady manner. The steady actuator was able to reattach the flow for angles of attack upto 19 degrees which is 4 deg past the normal stall angle and for unsteady case the reattachment of the flow was 9 deg past the normal stall angle. In the trailing edge the actuator was operated in steady manner and was found to produce same effect as a plane trailing edge flap.

The DBD plasma actuators were also seen to effectively control flow separation irrespective of their location on airfoil. Corke, Post, Jumper[21] applied the weakly ionized plasma for flow control in 72% x/C location of NACA 0009 airfoil. Chord and Span of the airfoil was 20.2 cm and 41.7 cm respectively. The Reynolds numbers used in their experiments were 180k and 36k. The angle of attack was also varied from -12 to 12 degrees. From the experiments, they found that plasma actuator increases the lift coefficient over the full range of angle of attack, similar to adding camber. Huang et.

al[22] incorporated dielectric barrier plasma actuator in a linear cascade of Low pressure turbine blades. They used Pak B blade profile and experimental conditions at a chord Reynolds number of 50k, free stream turbulence level 0.08 to 2.85%. Two x/C locations of plasma actuator were examined, 0.4 and 0.675, where the location of separation was at 0.70 x/C. Actuator on both chord locations could affect the separation, although the actuator in the downstream position, closer to the separation location was more effective. Post [19] et.al also performed experiments with on NACA airfoil with plasma actuators placed at the leading edge. In their experiments they observed plasma actuator was successful in enhancing lift for free stream flow up to 20 m/s.

Although plasma actuators have been successful as a flow separation control device, they are more successful in low speed flows. Post et. al[23] applied plasma induced separation control mechanism in NACA (663-018) airfoil. The airfoil was operated over a range of free stream velocities from 10 to 30 m/s giving a chord Reynolds numbers from 77k to 333k. They found better performance for plasma actuator operated for 10 m/s then the one operated at 30 m/s. The actuators were found to reattach the flow 8 degrees past the stall angle. Hultgren, Ashpis[24] et. al experienced separation delay for flat plate using plasma actuators. They varied the Re_c from 50k to 300k and free stream turbulence intensity of low (0.2%) and high (2.5%). Their results indicated that the actuator performance results in rapid reattachment. However, in their case, the low speed application of plasma was more successful in delaying flow separation. Greenblatt et. al [25] investigated the influence of DBD actuator for leading edge separation in flat plate and Eppler E338 airfoil. For their experiments they used Kapton dielectric and varied the frequency and voltage for

different plasma effect (3kHz < f_c < 10kHz and 6kVpp < V < 10 kVpp). The actuator was operated in steady and pulsed mode over Re of 3k to 9k. For Re of 3k case, they achieved C_L which is 43% higher than that of 9k.

Plasma actuators have not been able to influence the flow separation observed in high speed flows. Post et. al [26]studied the effectiveness of single dielectric barrier plasma actuator in high speed, natural laminar flow HSNLF(1)-0213 airfoil. The 10KVp-p actuator was simulated an aileron-up or trailing edge flap upward deflection at M=0.1 (Re=2.92X10^5) and M=0.2 (Re=5.84X10^5). The angle of attack is varied from -2 to 16 degrees. The results show that in both cases the C_L distribution over the angle of attack was largely identical.

Incorporating multiple plasma actuators was able to produce better separation control in different studies. Goksel [27] et. al incorporated plasma actuator in Eppler E338 airfoil. A total of 12 pairs actuator with tinned copper electrode and Teflon dielectric was employed in the suction surface of the airfoil. The flow was varied from 26k to 79k and angle of attack from 0 to 25 degrees. The found for Re 39750 the actuator produced lift increment upto 129% for α = 16 degrees. Jolibois [28] et. al performed flow measurements on NACA 0015 airfoil with and without plasma flow control at different free stream velocities. The DBD actuators had aluminum as electrodes and PVC as dielectric. A total of seven actuators with similar configuration were placed in the suction surface of the airfoil covering 30% to 78% of the entire chord. For Re = 40k they experienced a complete elimination of separation upto 17 degrees angle of attack. They also observed that with locating the actuator close to the separation point the electrical power for eliminating flow separation can be reduced

upto 25%. Although their work investigated the plasma actuator performance for a certain flow, their work did not explain how the plasma actuator has been placed on top of the airfoil suction surface. It has been observed our research that the method of actuator placement can influence flow separation of the airfoil.

Plasma actuators were found in other configurations than their flat plate arrangement as shown in Figure 1.1. Santhanakrishnan[29] et. al performed an experimental investigation on novel plasma actuator design consisting annular electrode orientation forming a circular configuration. The actuation cycle was studied in steady and pulsed condition. It was found that the plasma resembles a synthetic jet behavior. The pulsing frequencies were 1Hz, 10 Hz, 100 Hz and steady actuation. The maximum velocity obtained in quiescent flow was at 24 ms time and the velocity was over 100 cm/s.

Plasma performance was also observed at low pressure condition. Bottelberghe [30] et.al performed experimental investigation to observe plasma performance when pressure was gradually dropped from atmospheric pressure of 30 in Hg to 14 in Hg. They found an increase in plasma penetration and power consumption in 14 in Hg. The power consumption increased about 14% during the pressure drop. However, they found a thrust of nearly 0.012 N/m. The thrust falls in the range of thrust required for altitude control of micro satellite. It was reported by Bayt [31] et.al that the micro satellites currently weight 1-50 kg and produce a thrust of nearly 1 mN. So plasma actuators can be used to generate thrust needed for altitude control of micro satellites.

2.2. Blowing Flow Control

The Blowing Flow Control employs additional momentum in the boundary layer of the flow. Blowing a thin jet upstream or in the separation region increases the energy by replacing the low momentum fluid near the wall. The jet influences the velocity profile of the boundary layer and free stream is not largely affected.

The standard measure of momentum addition by blowing is the ratio between the added momentums to the total momentum of the flow. This ratio is called the relative momentum addition which was first introduced by Poisson-Quinton and given the symbol C_μ. The parameter is defined by the equation:

$$C_\mu = (\rho_j U_j^2 H)/(0.5 \rho_\infty U_\infty^2 L)$$

where, H is the slot height, and L is a reference length, ρ is the fluid density, U_j is the amplitude of the velocity at the jet exit, and the subscript "∞" indicates "freestream".

Although C_μ is the most popular way of quantifying the amount of blowing in flow control, Mc Auliffe[32] et. al introduced blowing in terms of blowing ratio B. The blowing ratio B is $U_{j\ max}/ U_e$ where U represents velocity, subscript j and e represents blowing channel and freestream respectively.

Similar to plasma actuator flow control, blowing flow control can also be performed in steady and unsteady operation. They were found effective in separation control in both conditions. Their performance also depends on the amount of momentum being injected. Blowing location was also fixed in all experiments. Weaver [33]et. al incorporated upper surface blowing to suppress stall in Boeing-vertol VR-7 airfoil. Steady and pulsed blowing was applied to sinusoidal pitching airfoil described by $\alpha = \alpha_m + 10^o \sin\omega t$. Tests were conducted at Re 100k and pitch oscillations with α_m =

10° and 15° and frequency range of k=0.005 to 0.15 were examined. Blowing conditions varying from Cμ=0.003 to 0.66. All these cases produced blowing that was capable of improving lift and avert dynamic stall. Weaver[34] et. al also performed strong steady blowing for dynamic stall control with blowing rates of Cμ=0.16 to 0.066 and found at Cμ=0.16, steady blowing prevents the leading edge separation bubble at several test points. It was seen higher Cμ value resulted in better separation control. Culley[35] et. al applied active flow control by means of blowing in the suction surface of stator vanes in a low speed axial compressor. Cμ = 0.002 to 0.028 was used with frequency of 280 Hz and 1800 Hz. Injection from the suction surface produced a reduction in separation on the vanes where separation was experienced before by increasing vane stagger angle by 3 degrees. Wong [36] et. al used NACA 0012 to find effective blowing location for flow control purposes. Re was fixed at 125k and angle of attack was varied from -20 degrees to +20 degrees. Experiments were performed at three different blowing positions (x/C= 0, 0.25, 1) at Cμ = 0.197 for lift augmentation. All the experiments produces that lift significantly higher with blowing when compared to the not blowing cases. Of the experiments most effective blowing location was found to be at 0.25c.

Higher blowing ratio was more successful in flow separation control the lower blowing ratio. In studies performed by Mc Auliffe[32] et. al at low pressure turbine cascade, steady blowing was used to control separation characteristics of turbine airfoil of Pak B profile at Re 25k and 50k. For Re of 25k flow, blowing ratio higher than 1.0 was needed to eliminate stall. At a Reynolds number of 50k, they observed a significant reduction in the profile loss.

Seifert and Pack [37] performed experiments at NACA 0015 airfoil with varying $C\mu$ from 0.0 to 0.100 in Re_c of 15k and α from -2 deg to 4 deg. The blowing was incorporated at x/C= 0.7 location and was run at both steady and oscillatory manner. They found that both steady and oscillatory blowing is capable of eliminating separation and jet momentum coefficient ($C\mu$) of at least 0.002 was needed to have any influence in boundary layer. However, achieving a high $C\mu$ value of 0.002 could be challenging for every airfoil since in $C\mu$ physical parameters such as slot height and characteristic length is also involved. If the blowing slot opening is thin, then it will require several times higher velocity than the freestream as blowing velocity. However, getting that $C\mu$ value is difficult and would require powerful compressor. In their experiment they used a pressure source which was powered by a motor of 1500 hp. This is an expensive and heavy device which is not suitable for flight operation. Carter [38]et. al used boundary layer suction blowing to improve aerodynamic performance to high turning compressor stator. They designed a suction blowing configuration where massflow removed from the boundary layer suction was added to the supply massflow, and the resulting combined flow is used for blowing on the suction surface to control separation. Experiments run at Re of 200k and motive mass flow of 1.6% suggests the effectiveness of the configuration with a maximum reduction of 65% in the baseline (no flow control) loss coefficient. All cascades were at zero degrees of angle.

Blowing techniques were also very effective in high speed compressible flows. Mc Manus and Magill[39] studied the separation control in incompressible and compressible flow using pulsed jets. They tested a NACA4412 airfoil section at

different velocities (M = 0.3, 0.4, 0.5). For M = 0.3 flow, they found a 11% increase in lift when blowing was used.

2.3. Objectives and Goals of the Current Study

The review of literature in the preceding sections has further revealed a clear picture about the challenges and limitations involved in DBD actuator and Boundary layer blowing flow control approach. Integrated plasma with blowing can eliminate these major drawbacks and result in a versatile as well as robust flow control method. Considering these issues, we present the objective and goals for the current study:

1. To understand how the Combined Plasma and Blowing configuration will produce high control authority and wide application.
2. Application of The Integrated Flow Control into well studied separation flow control of airfoils

To fulfill the first objective, a test setup was constructed with integrated approach. In the setup, blowing was simulated as vertically fired jet and plasma actuator was placed in the periphery of the blow opening. The flow control was characterized in still air.

To fulfill the second objective, NACA 0025 airfoil was used. Blowing mechanism was incorporated in the airfoil without changing the exterior shape. The airfoil was placed into two different free stream flow condition at 10 degree angle of attack. Since plasma actuators were successful in low speed conditions, the free streams of 3 m/s and 4.5 m/s have been studied. Blowing is set to $C\mu = 0.0005$ for 3 m/s free stream and to $C\mu = 0.000263$ for 4.5 m/s freestream. Along with blowing, plasma

actuator was also turned on to experiment the combined affect. The performance of the integrated approach was compared with other conventional flow control methods.

CHAPTER 3. EXPERIMENTAL SETUP & PROCEDURE

In this chapter, information is presented about the equipments used in this research. The chapter also describes the procedure involved in establishing the experimental facility and is divided into two sections. Section 3.1; describes the experimental facility which will be followed by section 3.2 where equipments used in this research is described. In section 3.3, experimental setups are shown and in section 3.4 experimental procedures are explained

3.1. Experimental Facility

Windtunnel: The experiments were conducted in a FLOTECK 1440 low speed, low turbulence wind tunnel located in Thermal and Fluids lab of NDSU. The experiments performed in the windtunnel were the airfoil investigations performed in the Application of Integrated control phase. The open-circuit windtunnel was equipped with a 30.48 cm × 30.48 cm × 91.44 cm (12 in × 12 in × 36 in) long test section. In order to reduce the turbulence, honeycomb flow straightener and conditioning screens were included in the settling chamber of the tunnel. A 4:1 contraction followed the settling chamber. The tunnel was powered by a variable speed 2 hp motor and the motor was equipped with a 24 inch composite blade adjustable pitch fan. A Parker 650 Volt AC drive controller was employed for speed control of the motor i.e. wind tunnel. Free-stream velocities can be varied from 0 m/s to 330 m/s by adjusting the motor setting. With the current motor setting, the speed could be varied from 4 m/s to 33.5 m/s.

Plasma Actuator: The plasma actuator used in this research consisted of an AC power source, an electric signal measuring device, an electrode and a dielectric material.

The AC power source consisted of a Function Generator (BK PRECISION 4017A 10 MHz), PLX 1802 Professional 1000 Watt audio amplifier (viz., input sensitivity: 1.28 Vr.m.s, frequency range: 20 Hz to 20 kHz and gain: 1: 20) and an Industrial CMI-6488 step-up transformer (viz., turns ratio: 1:137.5, input sensitivity: 80Vr.m.s and frequency limit: 20 kHz). This A.C. power source was capable of providing a voltage up to 20 kV at a frequency of 20 kHz. To measure the voltage and current of the plasma actuator, a PMK GMbh manufactured voltage probe (model PHV 4002-3 with x1000 Attenuation, 100 MHz, and 40kV peak pulse) and a Pearson current monitor (model 4100, sensitivity 1 volts/amp, max 5 amp rms) were used. The collected voltage and current data were transferred to the computer with the help of the LABVIEW (version 8.2) software and digital oscilloscope (model TDS 2012B 1 Giga Samples/sec; 2500 points record length).

Model: The model to be used for flow control experiments was the NACA0025 airfoil. The airfoil had a chord length of 15.34 cm (6 inch) and span of 27.94 cm (11 inch). As the plasma actuator and blowing circuit was employed in the airfoil model, a thick airfoil such as NACA 0025 was selected. Two airfoils of identical exterior shapes were constructed. The first airfoil was used for base line condition setup. This airfoil was equipped with pressure sensing ports incorporated in both suction and pressure surface. There were 16 different ports and each port was 0.03175 cm in diameter. The ports were guided from the suction and pressure surface all the way to the airfoil sides. The other airfoil was for experimentation of plasma- blowing integrated effect. Both the airfoils were modeled in SolidWorks and constructed by Metro RP with stereo-lithography process with layer thickness of 1/1500 inch. After the rapid prototyping

process, the outer blade surface has been cleaned and dried to ensure superior surface finish.

3.2. Equipment Used

Particle Image Velocimetry (PIV): The Particle Image Velocimetry (PIV) is an optical method used to obtain instantaneous flow properties of fluids. The fluid was seeded with tracer particles that follow the flow pattern of the medium, and was then illuminated with laser sheet and the flow field image was captured by a high speed camera with different frame settings. The captured images were then processed with cross correlation function in PIV processing software to extract information of the flow field.

In the current facility, the laser was pulsed in sync with TSI model 630046, a dual-head 50 mJ Nd-YAG laser from New Wave Research and PIV CAM 10-30 CCD camera which has 1008 × 1024 pixels of resolution. The CCD camera was able to capture each light pulse in separate image frames. The 2mm wide sheet forming lens spread the laser beam into a 2-D sheet. In both the cases, the flow field has been seeded with smoke particle diameter in the order of 1 micron. The seeding was generated from an American DJ Mini fog generator.

Pressure Sensors and Data Acquisition (DAQ): Pressure andvelocity measurements were completed with the differential pressure difference recorded in the computer using the Pitot static probe, Omega Differential pressure transducer and a DAQ system. The diameter of the pitot probe was 3/16 inch. The transducer had a range of 0-0.1 inch of water and uncertainty of 0.05%. The transducer gives a DC voltage output from 1-5 volts. The volts were calibrated to velocity via pressure differential

readings. Since the experiments were conducted in very low speed, and AVC -1000 pressure transducer calibrator was used to calibrate the pressure transducer. A voltage signal was acquired for the computer using a National Instrument Data Acquisition card (NIDAQ 6281) then converted to velocity readings through a vi written in LabVIEW. A traversing mechanism was used to traverse the pitot probe along the vertical axis of the test section. For traversing, the Velmex Traversing mechanism (MN-10-0100-M02-21) was used. This particular equipment was capable of producing 2.5 rev/sec and in each revolution it moved 5mm.

Hotwire Anemometry: Hotwire Anemometers were used to measure the minute disturbances present in the flow field. They are sensitive enough to capture the fluctuating component of the velocity (u'). In this research, experiments were performed using IFA 300 constant temperature anemometer from TSI Inc. The film type cylindrical sensor was capable of measuring minute disturbances in the flow field. The diameter of the sensor wire was 51 μ-m. The probe had a frequency response of less than 250 kHz. The system was connected to a computer by ADCWIN-4, DAQ card having a resolution of 12 bit. Calibration information for the Hotwire system can be found in Appendix A.4

3.3. Experimental Setup

In this section, the experimental setups are explained. Two different experimental setups were constructed. The first setup was used for the Characterization experiments and the second setup was used for the Airfoil application experiments.

Test Setup for Integrated Control: In Figure 3.1, schematic is presented of the setup where experiments were conducted for characterization of integrated flow control.

The Plasma actuator was mounted on a plasma base which was made of plexiglass. The circular actuator was used for these experiments. The plasma base was connected to a contained where flow was stored temporarily for stabilization. Initially, the seeding was collected to smoke storage by valve manipulation. Then shop air was used to generate a uniform cylindrical jet. The pressure of the container was measured as 2 Pa higher than the atmospheric pressure.

The Particle Image Velocimetry (PIV) technique was used to collect flow field information. For data collection, the PIV cam and the Laser source was oriented by forming a 90 degree angle between them. A 2D laser sheet was projected on the jet using the sheet forming lens and image was collected through the PIV cam.

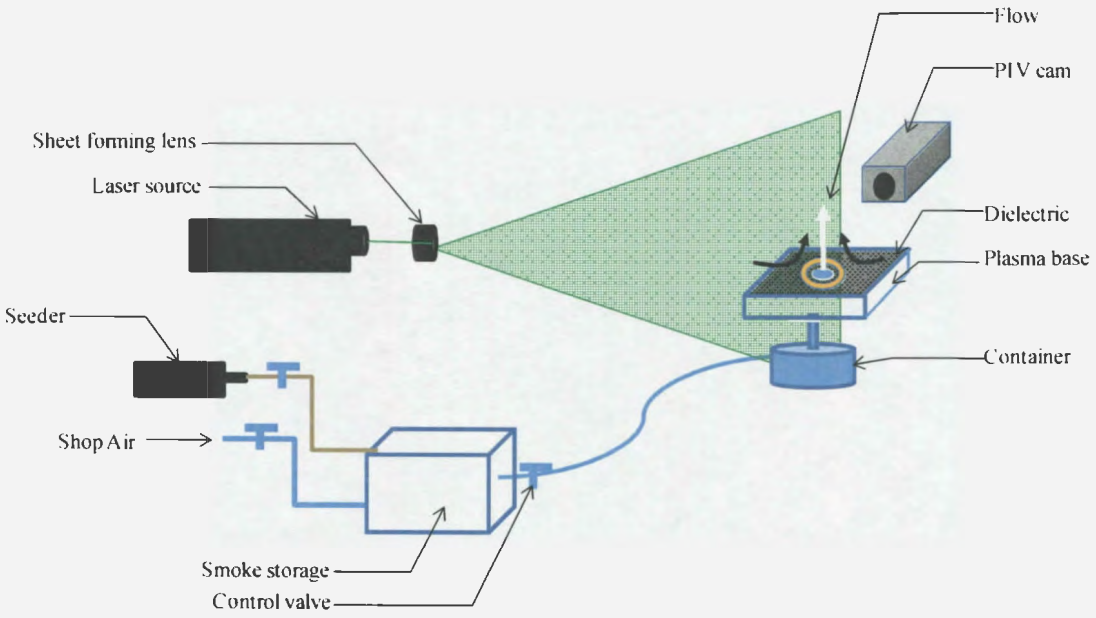

Figure 3.1. Schematic of test setup for integrated control

Application on Airfoil Experimental Setup: In Figure 3.2, schematic is presented for experiments performed on NACA 0025 airfoil in the windtunnel. For the exepirements, the airfoil model was placed in the airfoil and was set to desired angle of attack using the airfoil angle setup assembly. The flow was generated using the windtunnel fan and the flow was taken from the inlet located in the right of Figure 3.2. Flow conditioning was placed both in the tunnel inlet and the test section inlet. Seeding was initially taken in the smoke storage then shop air was used to create a minimal flow that was delivered in the windtunnel inlet. The tunnel was set at desired speed and the 2D laser sheet was projected on the airfoil. The laser illuminated the seeding particles and PIV cam was used to collect data. The tunnel also had a Pitot/ Hotwire sensor assembly to measure pressure and turbulence intensity data.

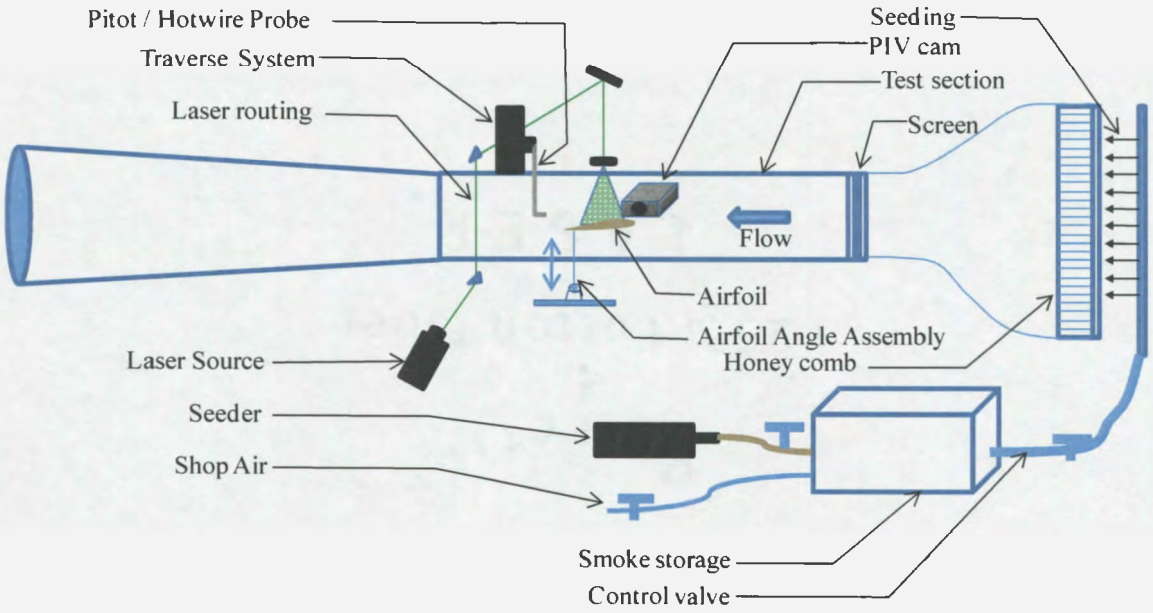

Figure 3.2. Schematic of application of integrated control setup

3.4. Experimental Procedure

In this section, the modifications and arrangements involved in developing the experimental facility is explained.

Windtunnel: The windtunnel was the first one to be used in any kind of aerodynamic research. Several modifications were completed on the windtunnel before any experiments were performed. To reduce the turbulence, honeycomb flow straightener and conditioning screens were included in the settling chamber of the tunnel. The screens contained small rectangular grids throughout the length of the chamber. The dimension for the smallest rectangle was recorded as 0.1 mm × 0.07 mm. The test section was included with removable plexiglass walls for visualization and a small window was also incorporated for easy access [Figure 3.3].

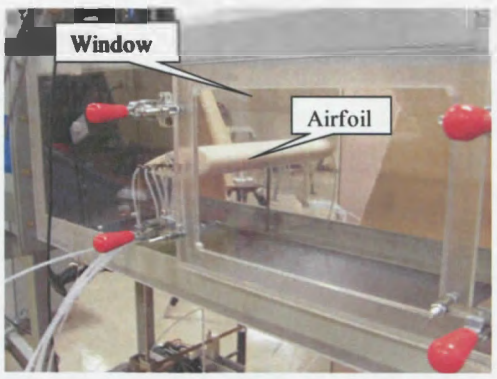

Figure 3.3. Windtunnel test section window

Since the windtunnel was new, it required a detailed investigation of flow stability, data repeatability and turbulence. Data was obtained with a pitot static probe equipped with a pressure transducer, PIV and Hotwire anemometer system. The pitot and hotwire probes were traversed manually in different spanwise horizontal positions and traversed in a vertical direction for a particular velocity profile. The total horizontal traverse was 17

cm. Data was collected at 36 different locations across this 17 cm wide area, each being 5 mm apart. For every single horizontal station, the pitot probe was traversed from the test section base to 250 mm upwards using a Velmex VXM stepping motor traverse system. Description of the experiments along with the results can be found in Appendix A.1.

Model Setup Procedure: The airfoil was mounted into the test section with mounting stick supports fabricated in the machine shop of the Mechanical Engineering Department, NDSU. In Figure 3.4, the leading edge support and trailing edge supports are illustrated. A rack and pinion mechanism was connected with a Vextra stepper motor that converted the rotational motion of the motor to linear vertical displacement of the airfoil tail. The vertical displacement of airfoil tail placed the airfoil in a desired angle.

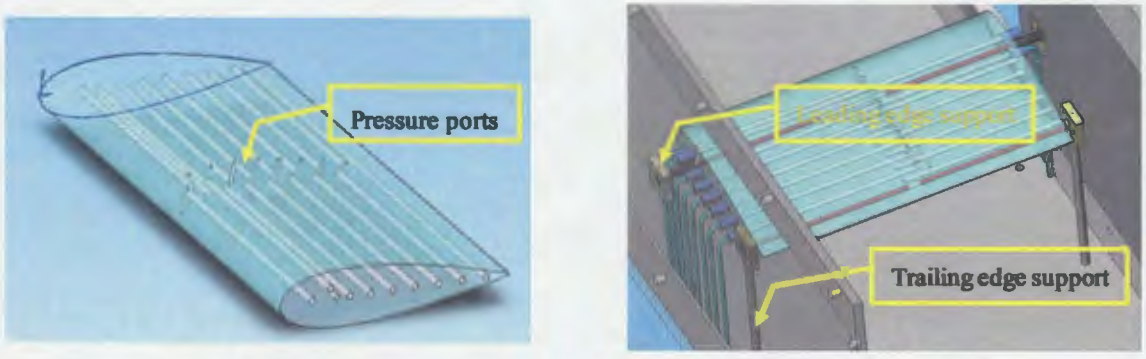

(a)Airfoil with pressure ports (b) airfoil mounted in windtunnel

Figure 3.4. Model setup

It has been found that a single step in the motor moves the airfoil at 0.45 degree of angle. The stepper motor is controlled with the help of National Instrument virtual

instrument (vi) written in LabVIEW. The experiments related to airfoil angle of attack setup can be found in Appendix A.2

Plasma actuator setup: The actuator used in the experiment has been constructed using a set of two copper tapes placed into opposite sides of a dielectric material. In Figure3.5 the schematic arrangement of plasma actuator used in this research can be seen. Two different kind of actuator had been used in current research. Figure 3.5 (a) represents the schematic of a rectangular plasma actuator configuration. From the Figure it can be seen that, the ends of the copper tapes are connected to the positive and negative terminals of a power source to complete the circuit. The copper tapes constructed the top and bottom electrodes needed for plasma actuation. The dimension of the copper electrodes was 76.2×25.4×0.0254 mm (3×1×0.001 inch). The dielectric material used in the study, Kapton polymide film, has a dielectric strength of 291 kV/mm and a film thickness of 10 mil. In Figure 3.5 (b) the schematic can be seen for circular plasma actuator. This actuator was used in the proof of concept experiment with the vertically fired jet. For this actuator, the electrode diameter was 6 mm. The dielectric used was the same. The electric signal generated from the function generator was of 0.9 Volts and it was transmitted to an audio amplifier for amplification where it was amplified 20 times to 18 Volts. The output from amplifier was fed to the transformer where it was raised 137.5 times to 2.475 kVolts rms. The positive and the ground terminals of the transformer are connected to the copper tape electrodes of the actuator. The output from the equipment is monitored using the Tektronix oscilloscope. The frequency was set at 8 kHz for all experiments.

The rectangular plasma actuator was mounted on the NACA airfoil. Since the incorporation of plasma actuator on top of the airfoil could possibly incorporate disturbing effect in the flow domain, investigations were performed to distinguish a 2D domain where disturbances were not present. A 2D domain is extremely important so that the end effects from the airfoil and the plasma actuator does not reach the experiment region of interest. To obtain a 2D flow domain, the pitot probe was traversed in horizontal and vertical direction with the airfoil placed in the tunnel.

The horizontal traverse was 60 mm each side from the tunnel test section and vertical traverse was 200 mm upward from the test section base. Results of the experiment can be found in Appendix A.5.

Particle Image Velocimetry procedure: In this research, PIV was the primary source of the experimental data. In the experiments, 1000 instantaneous images were captured during each set of PIV run. Since seeding was inconsistent, nearly 200 image frames were neglected and 800 images were processed using LaVision DaVis7 PIV processor. For processing multi pass mode was selected. The images were captured with a spot size of 32×32. In processing, the first pass was computed using 32×32 spot size then decreased to 16×16 with 25% overlap. A velocity filter of Vx = 0.0 $\pm$ 0.5 and Vy = 2.50$\pm$1.00 m/s was used in characterization tests of integrated control. For airfoil application experiments, the filter configuration was Vx = 0.3 $\pm$ 2.0 and Vy = 0.50 $\pm$ 1.00 m/s. Afterwards, the results were displayed using Tecplot and Spread sheet applications.

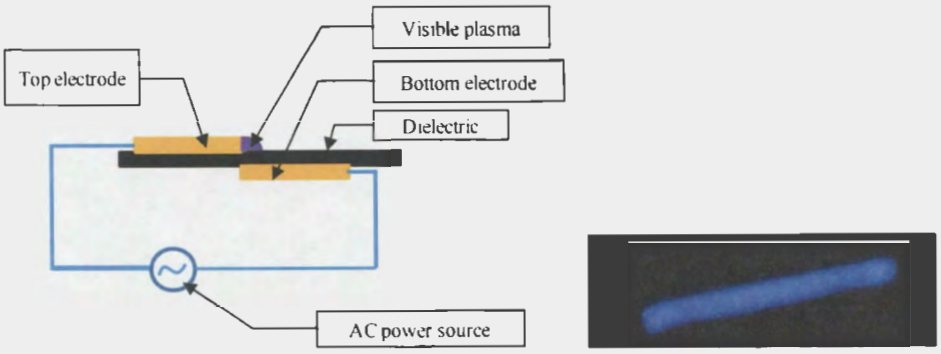

(a)Rectangular plasma

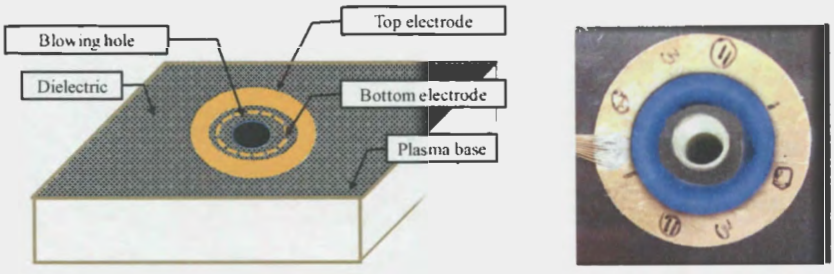

(b) Circular plasma

Figure 3.5. Plasma actuator configuration schematic

Blowing setup: For the experiments, very low energy blowing was used. At first, the seeding smoke was stored into a settling chamber. Then it is pressurized with shop air which was at slightly higher pressure (0.09 Pa g) than the atmospheric pressure. For the experiments, the blowing velocity is kept at 0.4 m/s. This velocity correspond to $C\mu$ = 0.0005 for 3 m/s and $C\mu$ = 0.000263 for 4.5 m/s. To achieve this blowing, the valves between the settling chamber and wall supply were adjusted manually and set to the specific position. From the settling chamber the pressurized smoke has been diverted towards the airfoil. The smoke enters the airfoil in both sides and comes out as a tangential flow over the airfoil suction surface. The blowing circuit inside the airfoil can

be seen in Figure 3.6. The channel has a 0.254 cm × 10.16 cm rectangular opening in the midspan of airfoil. The opening is created in such a way that the air would follow the airfoil suction surface tangentially. The opening was located at 0.25 x/C location of the NACA 0025 airfoil. Similar to the wintunnel flow field, an investigation was also performed for only blowing, to distinguish the 2D flow region. The pitot static probe was placed in three different horizontal locations along the blowing slot span. Details can be found in Appendix A.3.

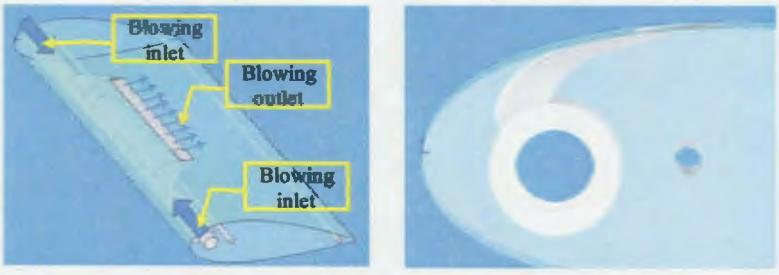

(a) Blowing flow channel (b) Blowing contour

Figure 3.6. Blowing configuration schematic of NACA 0025

CHAPTER 4. RESULTS AND DISCUSSION

In this chapter the results are presented for the integrated flow control research. The chapter is composed to two broad parts: Characterization of Integrated control as a proof of concept and Application of Integrated control on NACA 0025 airfoil. The chapter begins with section 4.1 where results are presented and discussed for the characterization and development of Integrated Flow Control method. In section 4.2, results are discussed for the Application of Integrated Flow control. Section 4.2 is sub divided into three more sections. In section 4.2.1 results are presented for placement of aerodynamic flow control on NACA 0025 airfoil, section 4.2.2 presents the results for plasma flow control and finally in section 4.2.3 results are presented for Integrated flow control.

4.1. Integrated Flow Control as Proof of Concept

The integrated blowing with plasma flow control was characterized by a vertically fired jet with plasma actuator placed around the periphery. In the experiments, blowing was simulated as a vertically fired jet and plasma actuator was placed to enhance the blowing energy. The top and bottom electrodes of plasma actuator constructed a no gap configuration. However, a gap of 6 mm from the hole end to the top electrode and 2 mm from the bottom electrode was kept in the final setup. In Figure 4.1 (a), the plasma actuator top electrode is seen along with the location where plasma was visible. The gap between the top electrode and original location of the hole is also visible. The hole and the bottom electrode had a gap of 2 mm. This gap was placed after the initial attempts had failed to generate stable plasma around the jet. The lower

amount of gap resulted in insufficient region for plasma augmentation. With lessened gap between the hole and electrode, the plasma could easily overcome the barrier through the opening resulting in a dielectric failure of the actuator. The current configuration however, produced stable plasma for all experimental conditions. For the experiments, the voltage rating of plasma around the circular hole was recorded as 2.475 Kilo Volts. The frequency was set to 8 KHz. The plasma appeared as a bright purple color ring around the hole and was only visible in dark room with lights turned off. [Figure 4.1(b)].

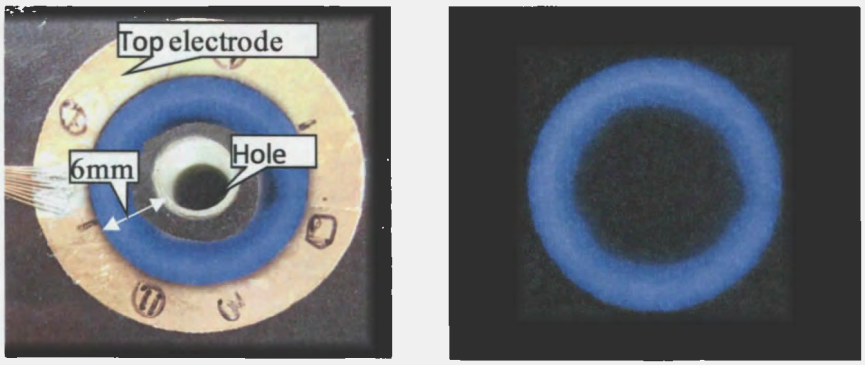

(a) (b)

Figure 4.1. Plasma actuator construction and appearance for cylindrical jet

A single jet with and without plasma activation was tested in different peripheral locations of the jet in current study. Figure 4.2 represents instantaneous PIV images of free jet. The 0.0 mm location of the jet corresponds to the center of the jet. Two completely different nature of the jet was captured in these set of images. The first image in Figure 4.2 represents the jet when it was at a perfectly vertical orientation. The other image, Figure 4.2 captured the jet when it was at the furthest deviation from its vertical orientation. A close observation of the jet revealed that the time interval between these two different orientations of jet was 0.6 seconds. The fluctuation was due

to external air disturbance. The jet was seen to be inclined in just one (left) side from the vertical orientation. The inclination of the jet was solely due to the reason of camera alignment with the horizontal axis. The angle was studied in Figure 4.2, the angle α was found same in magnitude of 4 degree for both cases. Figure 4.3 represents the average vector plot along with the speed contour plot for the current vertical jet orientation after a set of 600 images was processed. For results shown in Figure 4.3, the entire flow field was not taken into consideration. In Figure 4.2, a 15× 23 mm rectangle can be seen which is marked with white color. This was the area which was processed in DaVis to obtain results shown in Figure 4.3. It can be seen from the vector plot that the vectors are also inclined towards the left, which illustrates the fluctuating tendency of the jet and the camera inclined as explained earlier. It can also be inferred from Figure 4.3 that, the flow is parabolic in nature with highest velocity experienced at the center of the jet. As we move up along the vertical direction, the flow started to become stable and the high velocity region at the center started to diminish. From the speed contour plot, it can be observed that the velocity was quite stable along the span of the jet. The peak velocity has been reported as 1.84 m/s at the center of the jet. The current configuration will be intigrated with active plasma. Results are discussed later.

In Figure 4.4, an instantaneous PIV image of plasma active flow field in quiescent medium can be seen. The arrow heads indicate the direction of flow during the plasma active state. It can be seen from the Figure that the ionized gas pushed the stagnant air downwards towards the actuator and then gradually pushed it back in the upward direction. Similar to free jet, an area of interest was identified to be 15×23 mm for PIV image processing. This area was chosen in such a way that it captured the area

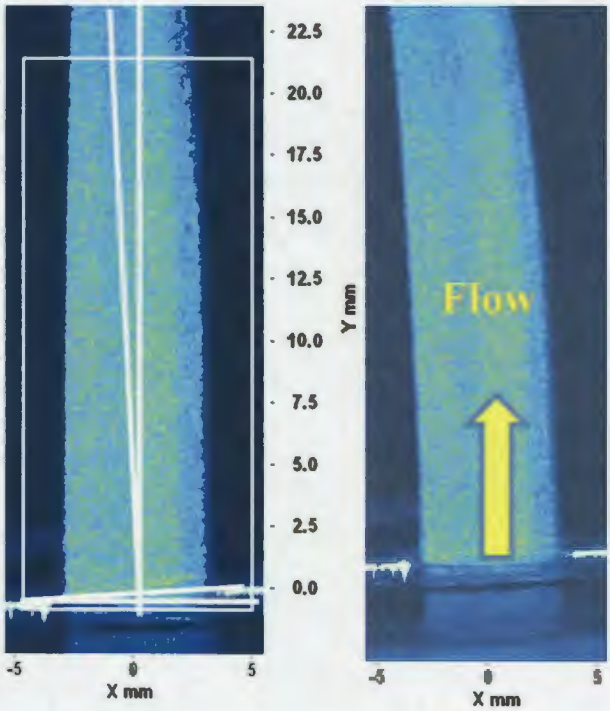

Figure 4.2. PIV image of cylindrical jet orientation

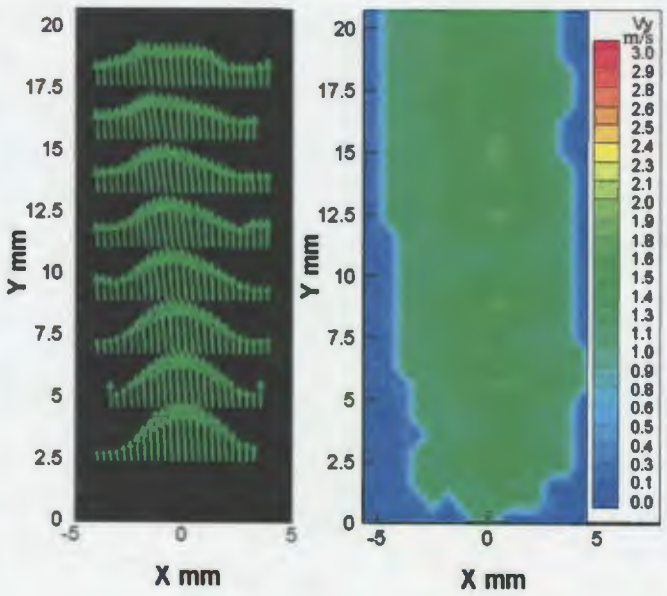

Figure 4.3. Vector and Speed contour for jet without plasma

the location of electrodes around the hole. As we were interested in investigating only the plasma influence in the jet flow, the entire flow domain was not taken into consideration.

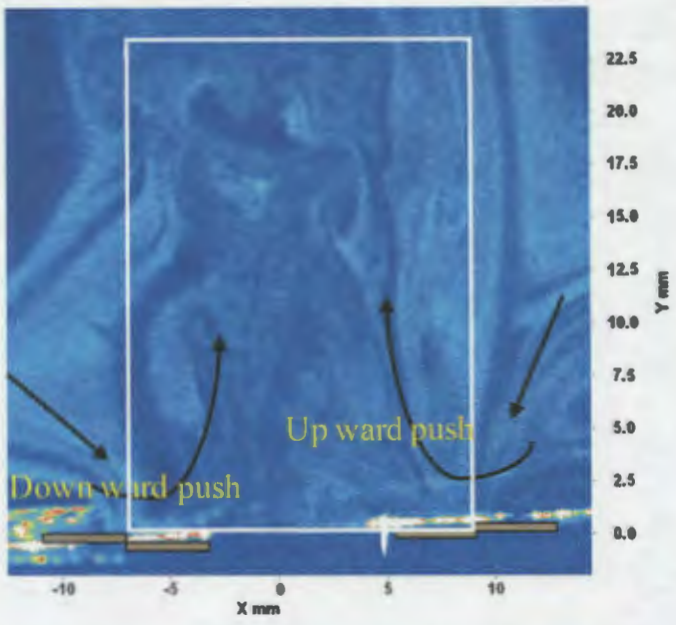

Figure 4.4. Instantaneous PIV image of active plasma in quiescent medium

The vector image and speed contour of plasma application in quiescent medium can be seen in Figure 4.5. The development of jet velocity can be observed from this image. The vector image shows the peak velocity was in the center of the jet. It also shows the parabolic nature of flow development. As the flow advanced along the vertical direction, the effect of plasma velocity starts to decrease similar to the free jet. A closer look in some of the vectors near the actuator would reveal the downward force of the plasma pulling the flow. The speed contour plot captured the different speed segments along the flow. The speed contour plot also indicates that the plasma enabled jet at quiescent medium is slightly inclined towards the left. This has been caused by the

slight inclination of the plasma base with respect to the horizontal coordinate. The reason for the inclination was the same as explained in the previous section.

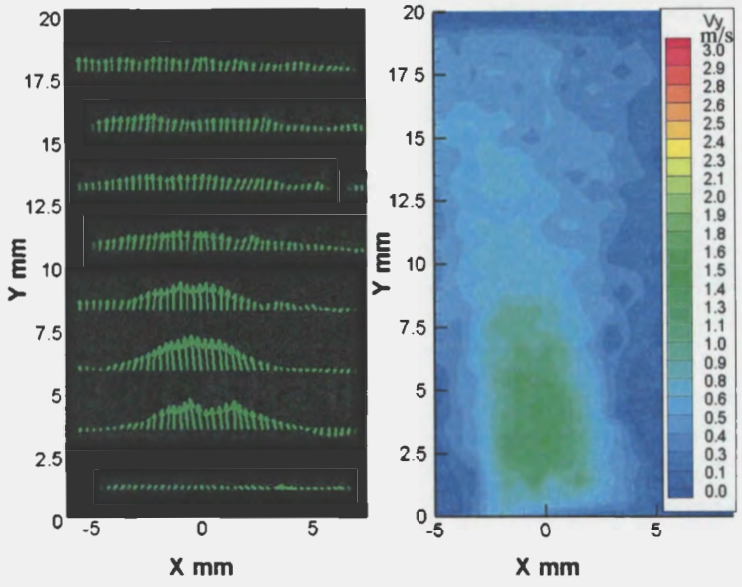

Figure 4.5. Vector and Speed contour for plasma in quiescent medium.

The streamlines on top of the speed contour can be seen in Figure 4.6. The streamlines was seen to move downward towards the actuator in the circle periphery then gradually go upward. Similar velocity distribution was also found by Santhanakrishnan et. al [30].

Once the flow information for free jet and plasma in quiescent medium was obtained, the next set of experiments concentrated in the investigation of combined effect of plasma and blowing. Three different locations were investigated along the periphery of the ring electrode for flow analysis. Each of the three locations was marked with straight line in Figure 4.7 to indicate the plane where the PIV measurements had been performed. The locations were important to gather an overall understanding of the flow domain.

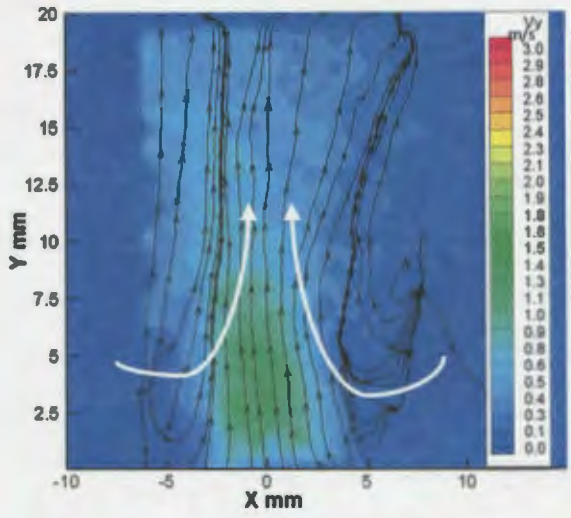

Figure 4.6. Streamlines of plasma in quiescent medium

The locations were named as location 0-0, location 2-2 and location 3-3. It was observed earlier by Santhanakrishnan et. al [30] that in the circular configuration, maintaining plasma uniform along the periphery was challenging. As the current condition was very similar to Santhanakrishnan et. al [30] condition, it has been decided to conduct investigation in more than one location to get better understanding of flow dynamics.

Figure 4.8 represents the PIV image taken in the first (marked as 0-0 in the corner image and highlighted in while line) location with the plasma enhanced jet. The plasma enhanced jet image was in clear contrast to the ones we have seen earlier. The jet still maintained the nearly cylindrical configuration. However, unlike the free jet, this jet was observed to be narrow than the earlier case. Also, the jet was no longer cylindrical throughout its entire length. The location of electrodes can also be seen.

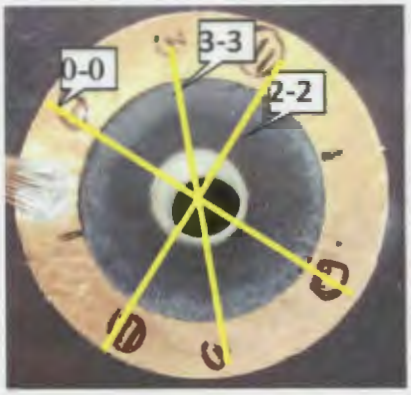

Figure 4.7. PIV planes considered for plasma investigation

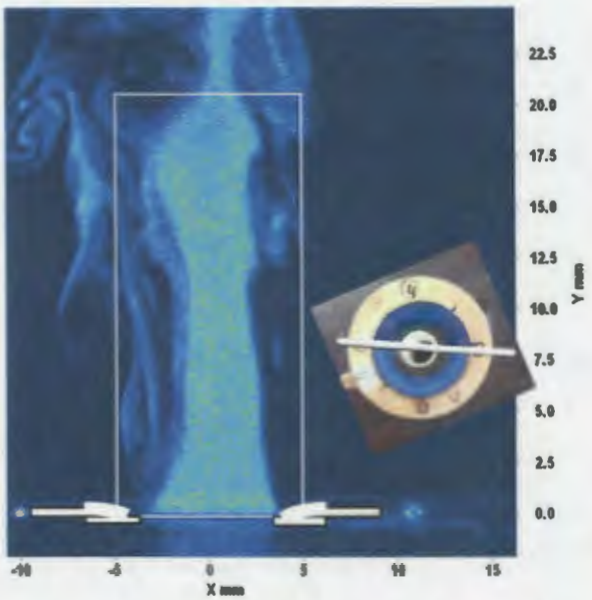

Figure 4.8. Plasma enhanced jet at 0-0 location

Figure 4.9 represents the vector and speed contour plot of plasma enhanced jet at 0-0 location. The vector plot captured some vectors inclined slightly towards the right instead of previously reported left side. This indicates the inconsistency of energy distribution of plasma along its periphery. Had the plasma been uniform throughout the entire periphery, the vector would show similar trends as was visible earlier. The contour plot reveals the velocity distribution along the vertical and horizontal

coordinate. The highest velocity was reported to be 2.75 m/s in the location 1.5 d higher than the base center, where d is the diameter of the jet hole.

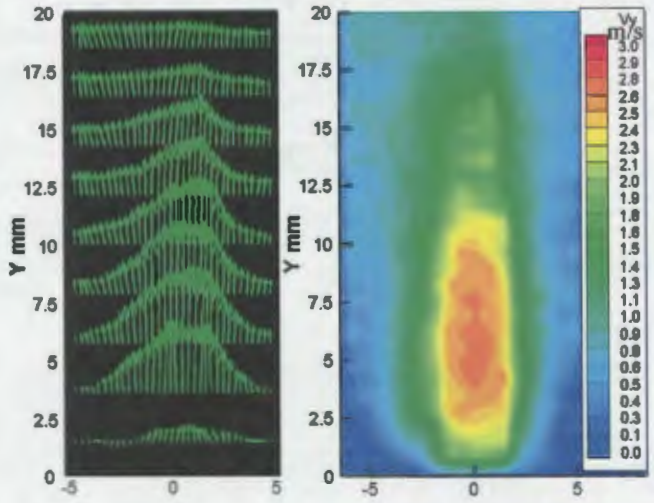

Figure 4.9. Vector and Speed contour plot of plasma enhanced jet at 0-0 location

The results for second location (2-2) investigated are represented here. The location was marked as straight line in the corner image of Figure 4.10. The Figure also captured the instantaneous behavior of plasma enhanced flow in the second location. The shape of flow was very similar to the first location flow.

The vector representation for the second location can be seen in Figure 4.11. This time, the vectors were found to be different than the first location. In this case the vectors were inclined towards the base. The jet shape was however, processing parabolic. Figure 4.11 also represents the speed contour for second location. Analyzing the PIV images it was determined that the maximum speed was experienced at the same 1.5d location of the jet The Plasma was influencing the entirety of the flow field. The maximum velocity was reported as 2.65 m/s for this location.

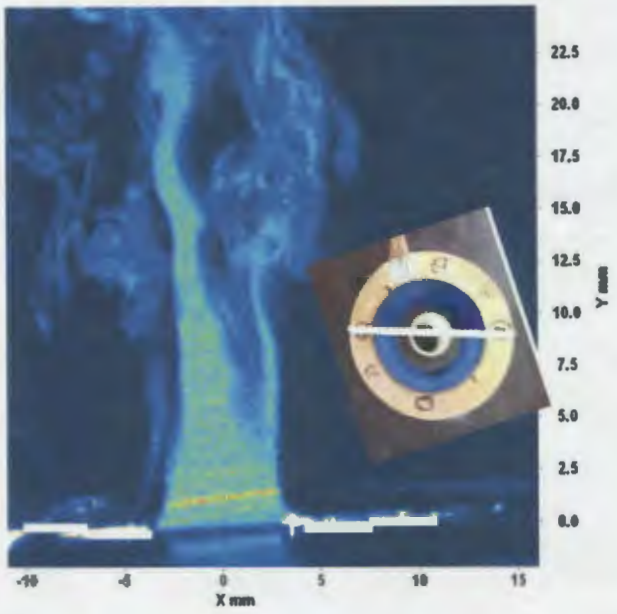

Figure 4.10. Instantaneous PIV image of Plasma enhanced jet at 2-2 location

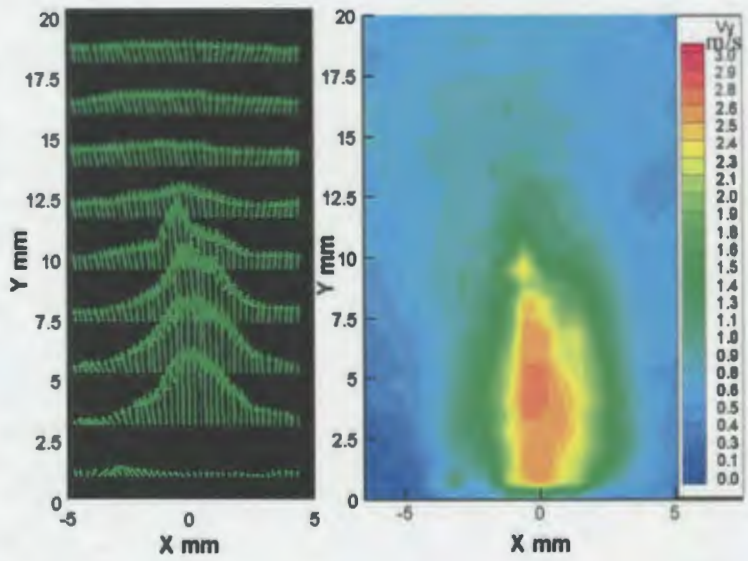

Figure 4.11. Vector and Speed contour plot for enhanced jet at 2-2 location

Although similar flow properties were obtained in the first two plasma locations, in the third plasma location better results were obtained when compared to the previous two locations. From the instantaneous PIV image in Figure 4.12 it can be seen that the

width of the jet has increased about 1 mm in each side. The jet is found to be oriented perfectly in the vertical direction. In the vector image for location 3-3, Figure 4.12, the vectors were found to be more prominent in the vertical direction and profile was seen to be more parabolic in nature. The speed contour [Figure 4.13] indicated a higher velocity in the center of current plasma induced jet. The magnitude of the maximum velocity was recorded as 3.1 m/s, the location was the same as the earlier which was 1.5 d upward from the base. The contour plot shows a deep color contrast at the center of the jet. It indicates a higher energy region of plasma in the current (3-3) location.

The results presented so far indicate that plasma combined with blowing had indeed incorporated momentum to the cylindrical jet. Quantitative information of this momentum addition was obtained through the velocity profile plot. Figure 4.14 represents the velocity profile for all configurations that have been discussed so far. The profiles were obtained at identical locations for each configuration. This location was 1.5d vertically upward from the base, d was the diameter of the cylindrical jet. From the Figure it can be seen that, peak velocity of free jet without active plasma was 1.84 m/s and peak velocity with only plasma in quiescent medium is 1.25 m/s. However, when both of them were combined together, the integration resulted in a higher amount of velocity i.e. 3.00 m/s. With this event, we can propose that the integration of plasma in free jet has resulted in a better performance compared to their individual contribution. As the free jet was at 1.84 m/s, the integration of plasma in the jet has added 1.16 m/s of velocity which is about 63.04 % increase in the velocity.

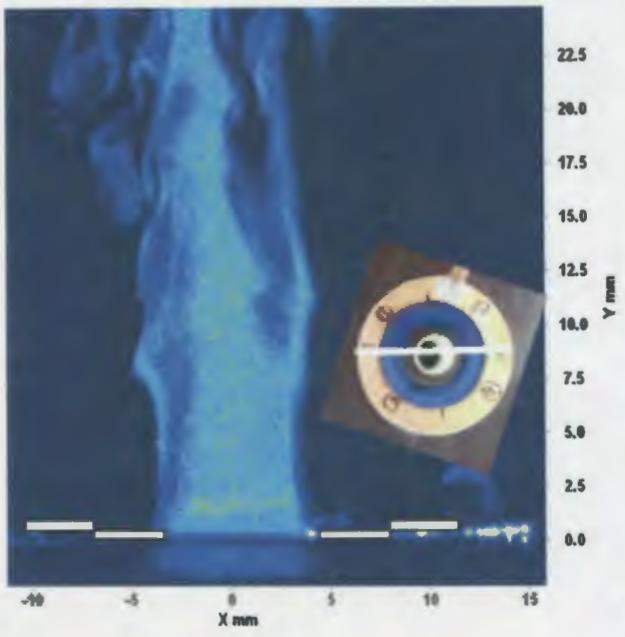

Figure 4.12. Instantaneous image of plasma enhanced jet at 3-3 location

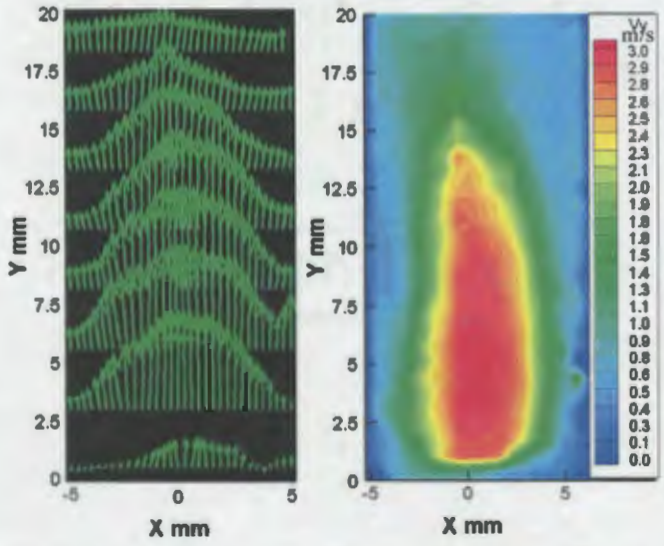

Figure 4.13. Vector and Speed contour image of enhanced jet at 3-3 location

The momentum addition by plasma 1.951×10^{-4} (kg*m)/s which is 165.7% increment compared to the momentum at 1.84 m/s jet. The results also indicate about 63% decrease in blowing ratio B. With this much reduction, the necessity of high

pressure source can be eliminated since plasma would produce the additional thrust needed for flow control. Plasma and blowing can also be operated individually which would result in a safer method of flow control. In low pressure applications, the blowing air would produce the negative oxygen and plasma would be able to produce enough thrust for altitude control.

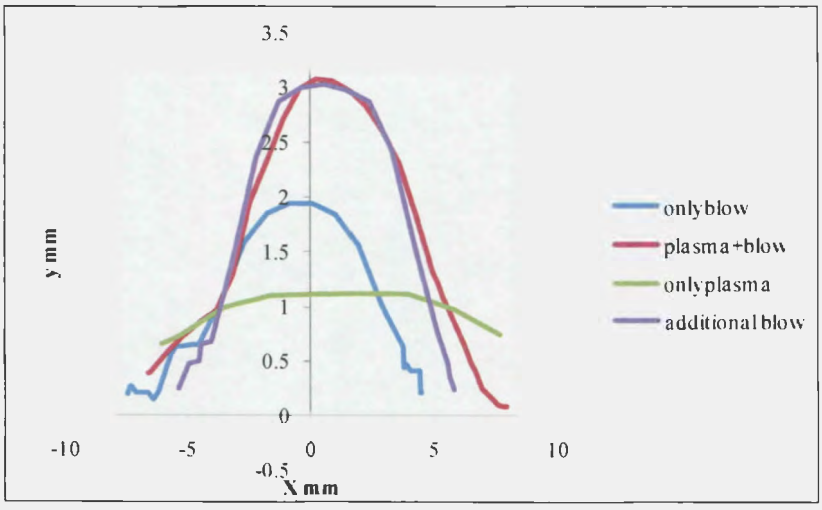

Figure 4.14. Velocity profile for different configurations of cylindrical jet

4.2. Application of Integrated Flow Control

After getting the results for characterization of Integrated Flow Control, we move on to investigate the Application of Integrated Flow Control. In this section results are presented for integrated flow control characteristics on NACA 0025 airfoil [section 4.2.3]. First in Section 4.2.1, results are presented for the investigation performed to determine an optimum location to place the aerodynamic flow control and finally, in section 4.2.2 results are presented for plasma flow control.

4. 2.1. Placement of Flow Control on NACA0025 Airfoil

Placement of flow control plays a crucial role in delaying or eliminating of flow separation. In this research, experiments were performed to determine the separation location of NACA 0025 airoil with varying angle of attack and freestream conditions. The investigations were performed in a qualitative manner by examining the real time PIV images taken through the PIV system. Based on the observations from this study, the location to place the aerodynamic flow control was determined. In the study, four angles i.e. 0,5,10,15 degree were tested initially in the windtunnel and separation for each airfoil was observed. The tunnel was run at two different freestream conditions i.e. 3 m/s and 4.5 m/s. It was found that for 0 and 5 degree angles, no separation was observed. For 15 degree angle, the separation was very strong and application of proposed flow control methodology would not be able to make any influence on it. However, for 10 degree angle of attack, the separation was moderate and incorporation of flow control could elminate or delay the separation. Based on the separation intensity, 10 degree angle to attack was chosen for investigation. Figure 4.15 represents a PIV image taken to illustrate the necessary terminologies involved in the current investigation.

Baseline separation locations were obtained with airfoil with no plasma actuator on it. Both 3 m/s and 4.5 m/s freestream conditions were tested. In Figure 4.16, an instantenous PIV image is presented for airfoil with both freestream conditions. In both images of Figure 4.16, the white rectangles indicate the area of interest for current set of experiment. Similar to previous set of experiments, the entire field of view was not taken into consideration. Only the region with ciritical flow features were investigated.

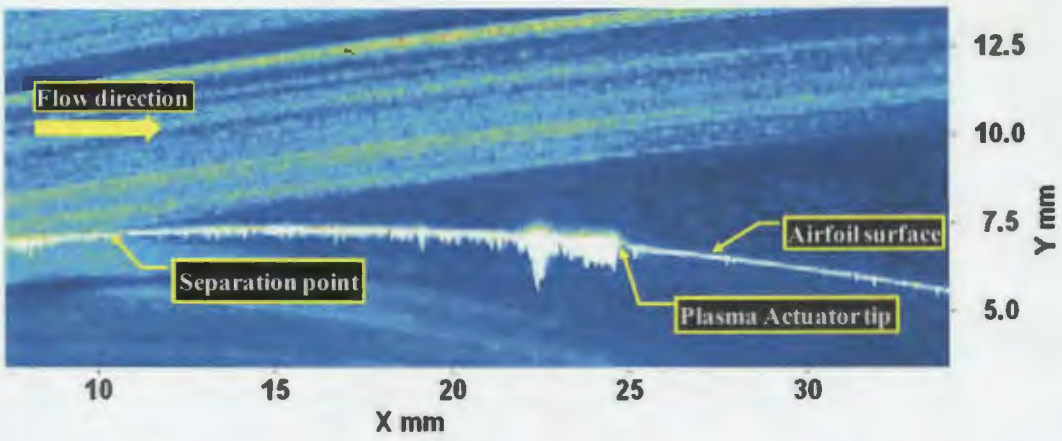

Figure 4.15. PIV image of flow over NACA 0025 airfoil

The PIV images presented in Figure 4.20 and Figure 4.21 correspond to the white rectangular area of Figure 4.16. Investigating the PIV images of Figure 4.16, the separation point for 3 m/s was found at 10.2% x/C location and for 4.5 m/s at 12.86% x/C location. It was calculated that, 1% x/C distance corresponded to 1.365 mm distance in the image for the experiments.

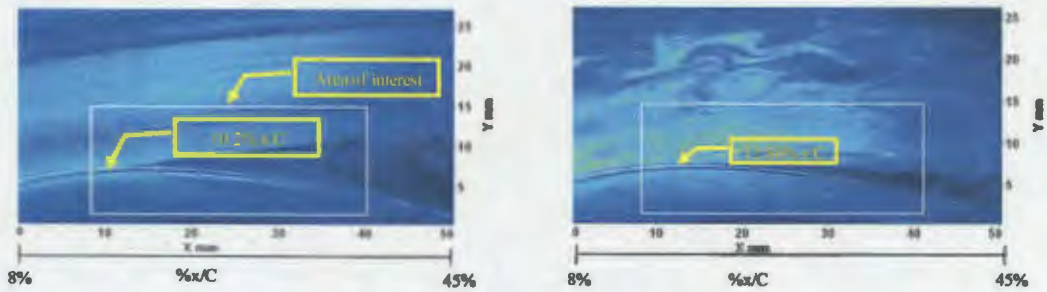

(a) 3m/s (b) 4.5 m/s

Figure 4.16. Separation locations at different speed

It was investigated afterwards if placing plasma actuator on the airfoil would alter the separation location. Since the airfoil would be run at two different flow conditions, the location to put the actuator was determined in such a way that it would

be applicable for both conditions. Considering the parameters, the actuator was placed at 15% x/C location of the airfoil and sepration characteristics was investigated in details.

Figure 4.17 represents PIV image of plasma actuator placed on 15% x/C location at different freestream conditions. It was revealed that although plasma actuator did not influence separation for in 3m/s, in 4.5 m/s, the separation location was altered. In 3m/s freestream condition, the separation was obtained at 10% x/C location this was very close to the baseline location of 10.2% x/C. For 4.5 m/s, the baseline location was 12.86% x/C, but the separation with plasma actuator placed was found at 11% x/C. In Figure 4.17(b), although it may reflect that applying plasma was not able to eliminate separation from the current image, after examining several images it was confirmed that the separation was indeed delayed to 21.43% x/C location. Since placement of plasma actuator on the airfoil has changed the location of separation, the actuator was placed in more than one location i.e. 20% x/C, 25% x/C to see if the location of actuator was responsible for altering the separation. Figure 4.18 presents PIV images for both freestream conditions with plasma actuator at 20% and 25% x/C locations. Although the change in separation location was not observed for 3 m/s, for 4.5 m/s freestream, there was major fluctuation in the separation location. In 4.5m/s, when the actuator was placed at 20% x/C location the separation shifted from 12.86% x/C location to 14.3% x/C location and when the actuator was placed at 25% x/C, the separation was shifted to 11% x/C location. As changing the plasma actuator location did not restore the baseline separation phenomena, later the actuator was glued over the airfoil surface at 25% x/C to make the actuator firmly connected to the airfoil. It was found that once the actuator

was glued to the surface, the separation occurred at 13% x/C location which was very close to the baseline location of 12.86% x/C.

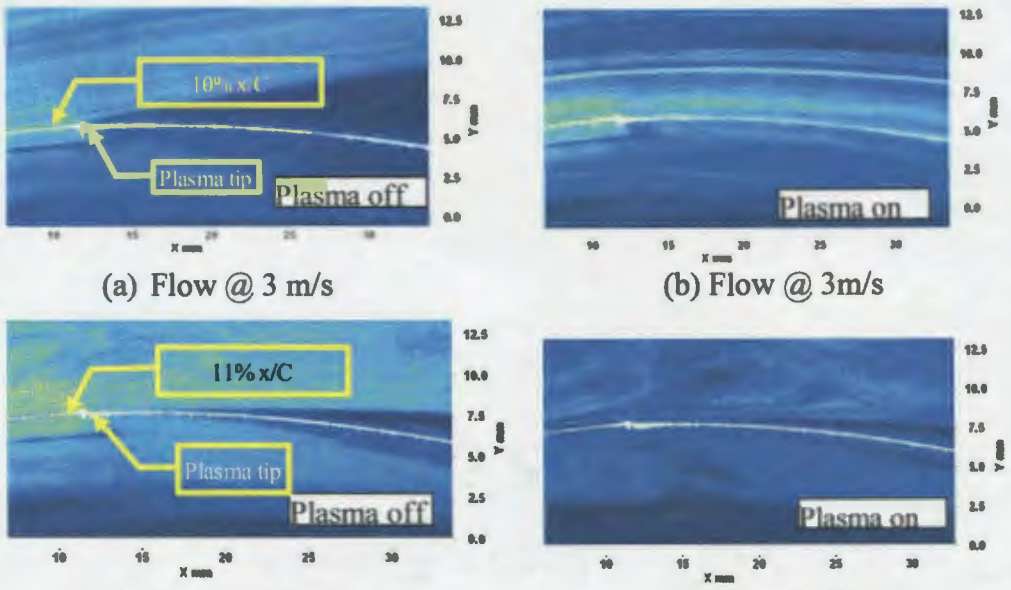

(a) Flow @ 3 m/s (b) Flow @ 3m/s

(c)Flow @ 4.5 m/s (b) Flow @ 4.5 m/s

Figure 4.17. PIV image of partial flow field with plasma actuator at 15% x/C

For the experiments performed afterwards, the actuator was always glued to the airfoil. Table 4.1 summarizes the findings for separation locations studied with active and not active plasma actuators. However, when the plasma actuator was turned on, irrespective of the chord wise locations, it was successful in delaying or eliminating flow separation.

The studies done so far indicate that plasma actuator placed in any location was effective in delaying if not eliminating flow separation. Among the locations 15%, 20% and 25% x/C, it was observed that when plasma actuator was placed in 25% x/C location, separation was delayed to the furthest downstream of the airfoil. Figure 4.19,

presents a graphical summary of different separation location when plasma actuator was placed in different x/C location and their influence on separation.

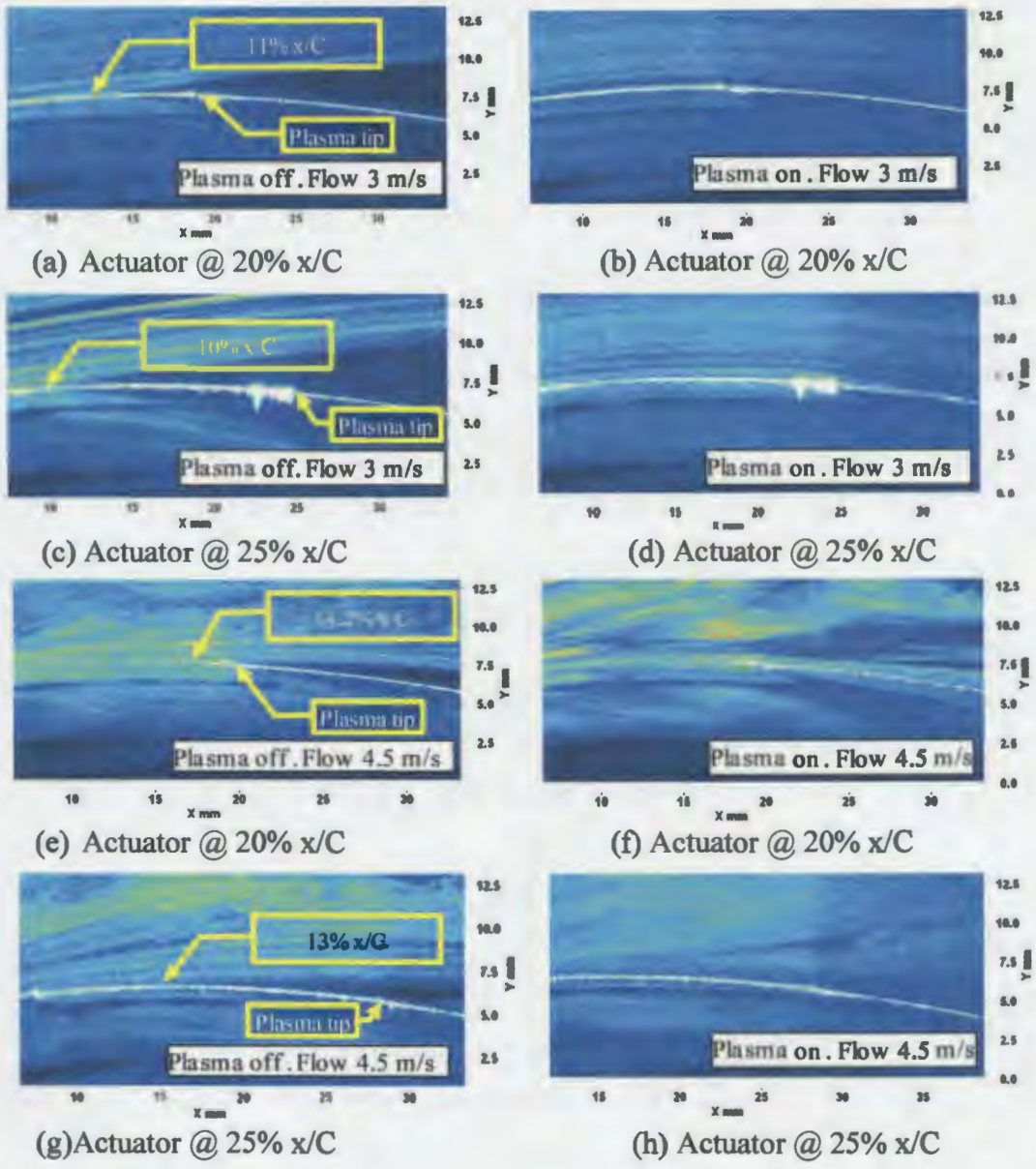

(a) Actuator @ 20% x/C (b) Actuator @ 20% x/C

(c) Actuator @ 25% x/C (d) Actuator @ 25% x/C

(e) Actuator @ 20% x/C (f) Actuator @ 20% x/C

(g)Actuator @ 25% x/C (h) Actuator @ 25% x/C

Figure 4.18. PIV image of partial flow field with plasma actuator at different location

Table 4.1. Separation location of NACA 0025 airfoil at different flow conditions

No.	Velocity (m/s)	Angle of Attack (deg)	Actuator location (mm)	Plasma	Separation location %x/C	Comments
1	3	10	No actuator	off	10.00	
2	3	10	0.15	off	10.00	
3	3	10	0.15	on	21.43	
4	3	10	0.2	off	10.00	
5	3	10	0.2	on	0.00	
6	3	10	0.25	off	10.00	
7	3	10	0.25	on	0.00	
8	4.5	10	no actuator	off	12.86	
9	4.5	10	0.15	off	10.71	
10	4.5	10	0.15	on	21.43	
11	4.5	10	0.2	off	14.29	
12	4.5	10	0.2	on	25.00	
13	4.5	10	0.25	off	10.71	no glue
14	4.5	10	0.25	off	13	glued

In case of 3 m/s freestream condition, when the actuator was at 25% x/C location, the separation was delayed till 29% x/C location and for 4.5 m/s freestream, no

separation was observed in the PIV image. Considering the encouraging results obtained with plasma at 25% x/C location, this location was chosen to be the location of aerodynamic flow control.

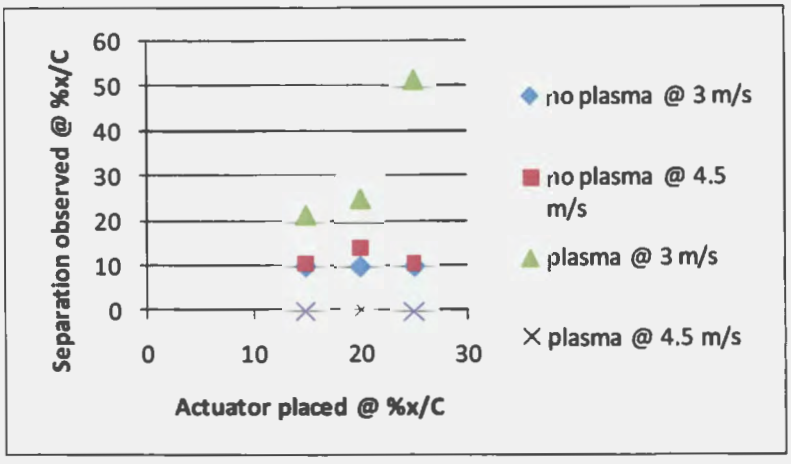

Figure 4.19. Separation location at different plasma actuator location

4.2.2. Results for Plasma Flow Control

Once the location of placement for flow control was determined, further investigation was carried with plasma flow control at 25% x/C. Results are discussed with the help of vector plots, streamlines and velocity profiles. In this study, the actuator was always placed at 25% x/C location. Figure 4.20 represents the vector plots for no plasma and active plasma conditions for 3 m/s free stream. From the Figure, it can be seen that the active plasma changed the flow to become more attached towards the airfoil surface. Figure 4.21 represents the streamline plot for the same flow condition. In the Figure, influence of plasma to make the flow streamlined is clearly visible. Similar results were also obtained for 4.5 m/s freestream. The results are presented in Figure 4.22 and Figure 4.23. The results are similar to the once obtained for 3 m/s.

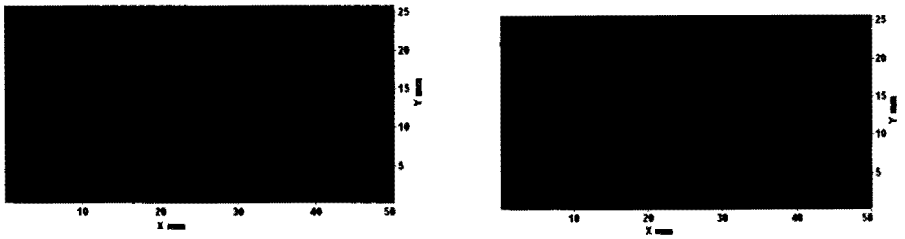

(a) Plasma off (b) Plasma on

Figure 4.20. Vector plot of airfoil at 3m/s and plasma actuator at 25% x/C

The plasma based flow control was also studied with the velocity profile plot extracted in different x/C locations along the airfoil chord. Three different locations were chosen i.e. 20%, 25% and 30% x/C locations where the profile was obtained.

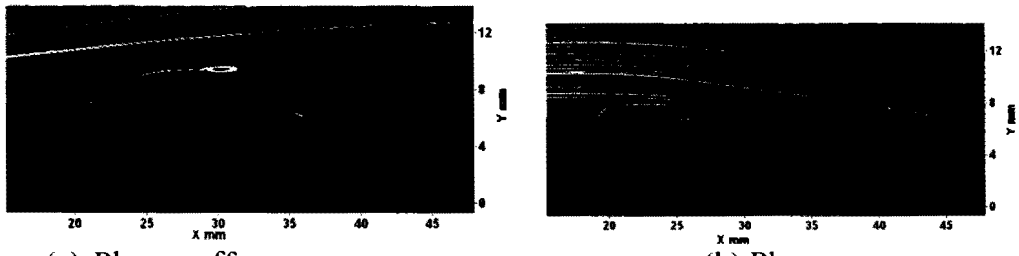

(a) Plasma off (b) Plasma on

Figure 4.21. Streamline plot of airfoil at 3m/s and plasma actuator at 25% x/C

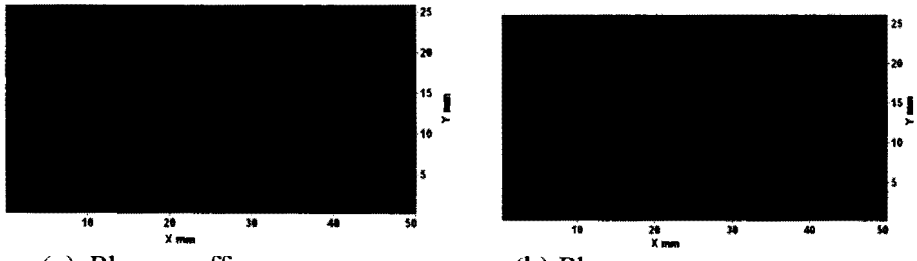

(a) Plasma off (b) Plasma on

Figure 4.22. Vector plot of airfoil at 4.5m/s and plasma actuator at 25% x/C

Figure 4.24 represents the velocity profile at 20% x/C location with and without plasma application for both of 3 m/s and 4.5 m/s freestream conditions. From the Figure, it can be seen that with the application of plasma, there had been a significant increase in near wall velocity.

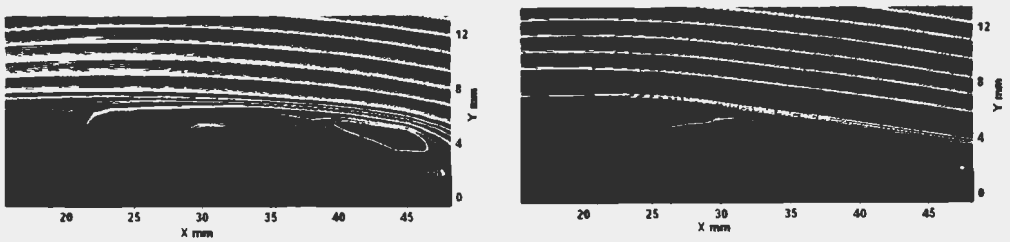

(a) Plasma off (b) Plasma on

Figure 4.23. Streamline plot of airfoil at 4.5m/s and plasma actuator at 25% x/C

The velocity increment was higher for the 3m/s compared to 4.5 m/s freestream. For the 4.5 m/s freestream, we can see from the plot that velocity recorded was nearly 8 m/s which was higher than originally 4.5 m/s. This velocity was higher due to aero dynamic shape of the airfoil. As the air passes over the airfoil suction surface it started

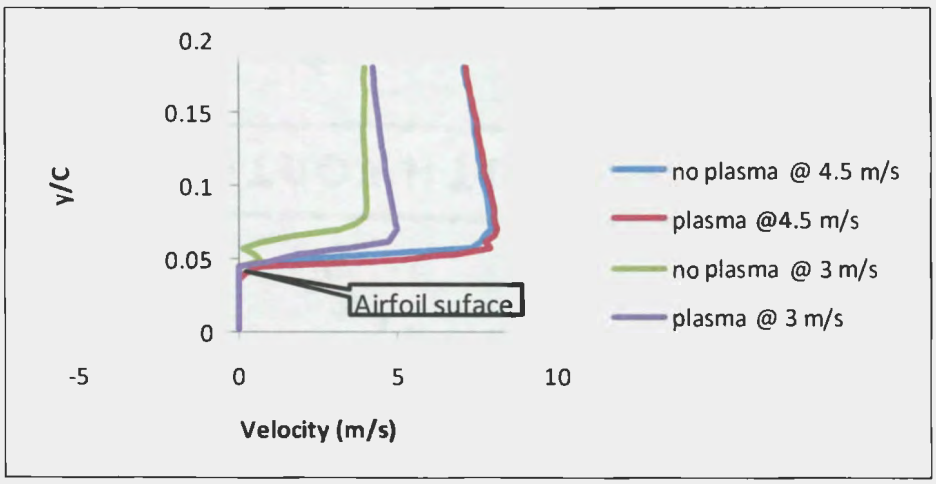

Figure 4.24. Velocity profile at 20% x/C location with and without plasma

to experience low pressure on the surface and that low pressure corresponded to an increase in velocity. The near wall velocity obtained with plasma based flow control was 0.133 m/s at 25.5 % x/C location. Similar velocity was obtained by Ramakumar [8] et. al, they obtained 0.5 m/s near wall velocity with similar actuation method at 1m/s

freestream. Jolibois [29] et. al and Balcer [17] et. al also obtained similar near wall velocity. Figure 4.25 and Figure 4.26 represent the profiles at 25% and 30% x/C location. From the Figures it can be seen that plasma was able to influence the separation of 3 m/s compared to 4.5 m/s. For 3m/s in both 25% and 30% case, the momentum addition was higher than 20% location.

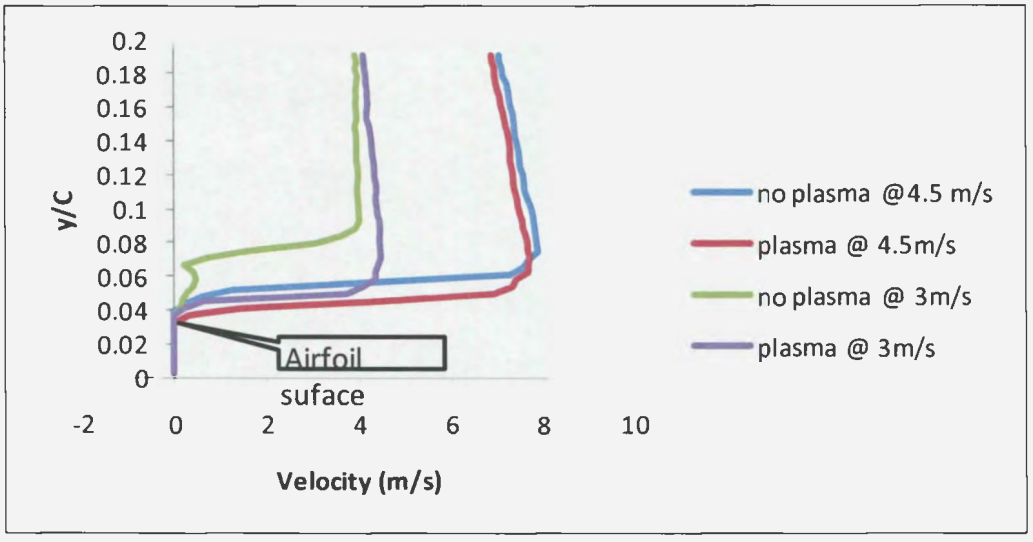

Figure 4.25. Velocity profile at 25% x/C with and without plasma

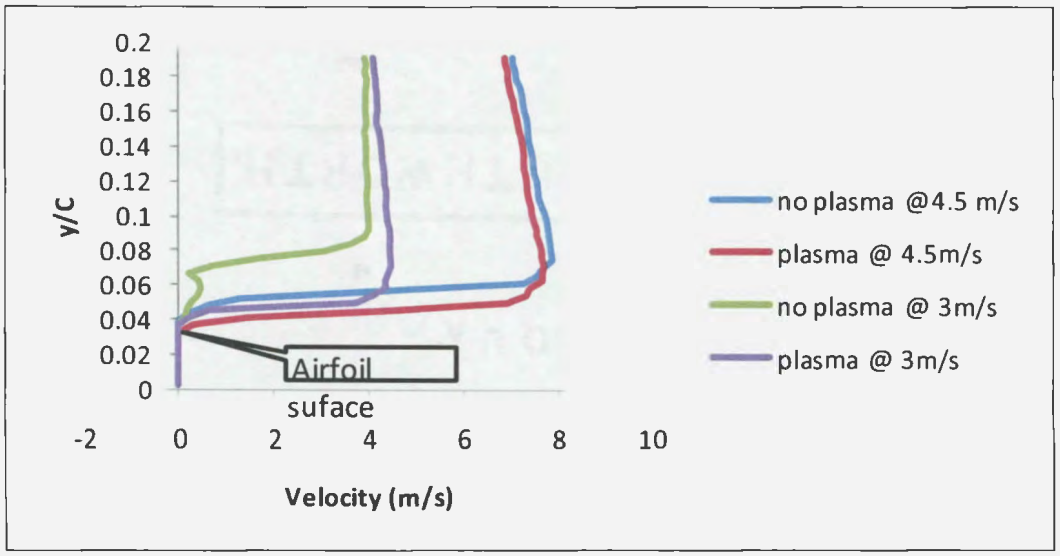

Figure 4.26. Velocity profile at 30% x/C with and without plasma

4.2.3. Combined Plasma and Blowing in NACA 0025 Airfoil

In the final stage of the research, the integrated plasma with blowing flow control was applied in NACA 0025 airfoil with blowing slot located at 25% x/C location and plasma actuator mounted in 25.5% x/C location. The results were obtained investigating the real time PIV image, Velocity vector plots, Streamlines, Speed Contours and Velocity profiles.

In these set of experiments, four different flow control parameters were chosen to investigate: Airfoil with no flow control, Airfoil with blowing, Airfoil with plasma and Airfoil with Integrated control. In blowing, the blowing coefficient, C_μ was used to be 0.005. The coefficient was determined with the equation of $C_\mu = (\rho_j U_j^2 H)/(0.5 \rho_\infty U_\infty^2 L)$, where H was considered as 0.254 cm, L was considered as 15.24 cm, U_j and U_∞ were considered as 0.4 m/s and 3.00 m/s respectively. The C_μ value of 0.0005 was significantly lower than the minimum value required observing a blowing effect. Culley [32] et. al reported that, C_μ lower than 0.002 was not capable to producing any influence in the separation region. However, since plasma would also contribute in the control method, it would be an interesting point to investigate, if such value of C_μ integrated with plasma could actually produce any effect. The other reason for having low C_μ was the physical parameters of the airfoil. The difference between the slot height H and reference length L was significantly larger in this case. However, the blowing ratio was also compared without incorporating the physical parameters of the airfoil. The value of U_j^2/ U_∞^2 was calculated as 0.0178 and value of U_j^2/ U_∞^2 performed by Culley [38] et. al was 0.176. This result indicates that, the blowing performed in the current study was significantly lower than the one used by Culley [38] et.al.

Figure 4.27 represents a PIV image of NACA 0025 airfoil distinguishing necessary features used in the current experiment. Figure 4.28 summarizes the results for current set of experiments. Figure 4.28 (a) represents instantaneous PIV image for flow over NACA 0025 airfoil when no flow control was used. The location of blowing and plasma is marked in the Figure. The separation location was also marked in the Figure. For this case, the separation was observed at 10% x/C location, which was concurrent with the earlier experiments performed. The separation of the flow is more vividly displayed in the vector plot illustrated in Figure 4.28 (b) and in the streamline plot in Figure 4.28 (c). A large separated region is visible right after the blowing slot location.

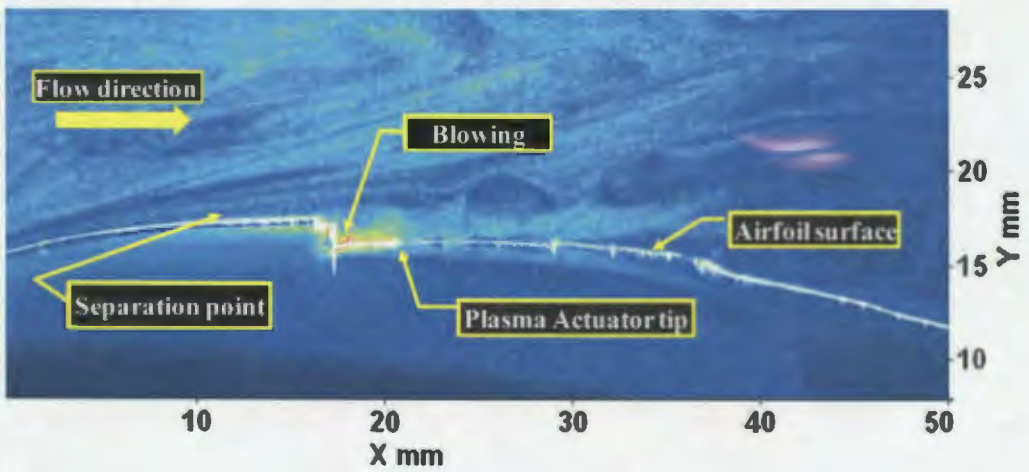

Figure 4.27.PIV image of NACA 0025 airfoil with integrated flow control

In Figure 4.28 (d), 4.28 (e) and 4.28 (f), flow field characteristics are illustrated where 3m/s freestream was incorporated with blowing of $C\mu = 0.0005$. Figure 4.28 (d) represents a PIV image of blowing flow control at 3m/s. In this particular case, blowing was found inconsistent. Instead of following the airfoil suction surface, for this case, the

blowing was lifted upwards towards the low pressure region of the airfoil. The Figure also clearly indicates that blowing was not sufficiently powerful to overcome the separation. Large voritices were seen even after the blowing flow control was turned on. The vector plot of blowing in Figure 4.28 (d) indicates that the blowing was able to incorporate some momentum in the separated flow but it was clearly not strong enough to delay the separation. The velocity profile got slightly changed when blowing was incorporated which can be seen in Figure 4.28 (e). The large vortices and separated flow can also be visible in the streamline plot at Figure 4.28 (f).

The results for 3m/s freestream with plasma flow control is presented in Figure 4.28 (g), 4.28 (h), 4.28 (i). Figure 4.30 (g), the real time PIV image of the flow can be seen. Unlike the blowing flow control case, here the flow was seen to be attached just about 1% x/C downstream of the actuator location. The large separation region was still present in spite of plasma incorporation which can be seen in the vector plot at Figure 4.28 (i). The Figure also captured the extent to which plasma actuator was able to delay the separation. The streamline plot at Figure 4.28 (j) shows a small piece of vortices initiating at the blowing slot opening and extending all way along the chord wise length.

The results for integrated control at 3m/s are presented in Figure 4.28 (j), 4.28 (k), 4.28 (l). In Figure 4.28.k, the instantaneous PIV image shows the blowing integrated with plasma. The extent along the chordwise length where the integrated control was influencing the flow can be seen from this Figure. In the vector plot at Figure 4.28 (k), the integrated control was seen to delay the separation more effectively than the previous two cases where only a single control mechanism was used. Similar results were also found in the Streamline plot at Figure 4.28 (l). The flow was seen to be

more attached and streamlined. However, a narrow separated region was also visible in the farthest downstream location of the airfoil.

Additional investigations were also performed with investigating the speed contours of different configurations explained so far to understand the overall flow field. Figure 4.29 presents the speed contour plots for all the flow control methods studied so far. The speed contour plots complement the findings of the vector and streamline plots. In Figure 4.28 Separation vortices were present afterwards the 35% x/C location of the airfoil. When the flow was incorporated with blowing of $C\mu$ =0.0005, the momentum addition was not strong enough to prevent the separation.
The Figure also indicates the upward lift of the blowing. The flow over the airfoil clearly did not become attached at all. Similar characteristics were also observed when the flow was incorporated with plasma actuator. Separation vortices can be seen in the region after 35% x/C. However, when the flow was incorporated with integrated flow control mechanism, the separation was largely delayed and flow had become more attached towards the airfoil surface.

The influence of the integrated plasma and blowing was also investigated with velocity profiles extracted in different x/C locations. The velocity profiles would be able to produce precise quantitative information about the benefits of integrated control. Three locations along the NACA 0025 airfoil chord was chosen to plot velocity profiles i.e. 20%, 25% and 35% x/C locations.

Figure 4.30. shows the velocity profile taken at 20% x/C location for 3 m/s free stream. The airfoil with no flow control, airfoil with blowing, airfoil with plasma and airfoil with plasma integrated blowing are the parameters that have been studied in the

current section. It can be seen from Figure 4.30. that any influence of any flow control was hardly evident. Since the 20% x/C location was upstream of the location, this location would not experience the influence of flow control to a great extent. In the velocity profiles, the profiles were extracted starting from slightly below the airfoil surface. Since we are interested in obtaining near wall velocity, this process was chosen. Flow control was meant to add additional energy in the near wall region of the airfoil, we were more interested to observe the development of flow vertically starting from the first position in the wall. In Figure 4.30, along with the profiles, the initial position of the airfoil is also marked with a label.

The second location velocity profile has been extracted was the 25% x/C location. Figure 4.31 shows the profiles extracted in that location for different flow control method investigated. From Figure it can be seen that the applied flow control methods was not able to incorporate any influence even at this location. Since influence was negligible, the near wall location of the profile was magnified in Figure 4.32 to have a closer look on the flow field. From the Figure it can be seen that the integrated approach was able to produce velocity in the near wall region where blowing was ineffective. The third location where velocity profiles were extracted was the 35% x/C location. This location was chosen since it was a downsteam location along the chord, it would be able to capture the influence of flow control better than other two locations. Figure 4.33 presents the velocity profiles different flow control methods studied in current research. The gradual development of the velocity profiles can be seen in this plot. The free stream was set at 3m/s. A careful look would reveal the combined plasma

and blowing affect has resulted in better separation control than the other techniques used.

The single plasma and single blowing was not able to make any influence in the separated flow region. However, when the plasma was integrated with blowing, it was able to make reasonable improvement in the separated flow. A magnified version of the influence of these two methods can be seen in Figure 4.34. The magnified plot captures a wide separated region in the near wall of portion of the airfoil even when the blowing was active. However, when this same blowing was integrated with plasma, it was able to eliminate that separation and made the flow attached to the airfoil surface. Velocity profile results indicate a 110% increase in near wall velocity at 35% x/C and 0.016 %y/C location with integrated control in place.

When the airfoil was studied at 4.5 m/s, the integrated control method was not able to produce any benefit. There were several factors which would possibly effect the flow phenomena studied for 4.5 m/s freestream. First of all comes the incorporation of blowing slot. Although experiments ensured that the blowing slot was located prior to the separation point so that the separation point is not disturbed by the blowing slot. However, the blowing slot could still influence the separated flow in the location after the blowing slot. A change in flow feature would require a changed flow control parameter to mitigate the separation. The turbulence intensity was another factor that could have influence in separation extent. As flow velocity was increased from 3 m/s to 4.5 m/s the turbulence intensity was changed from 0.33% to 0.51 %. The change in turbulence intensity may have influenced the flow greatly. More experimentation would be needed to clearly analyze the changing features of flow for 4.5 m/s free stream.

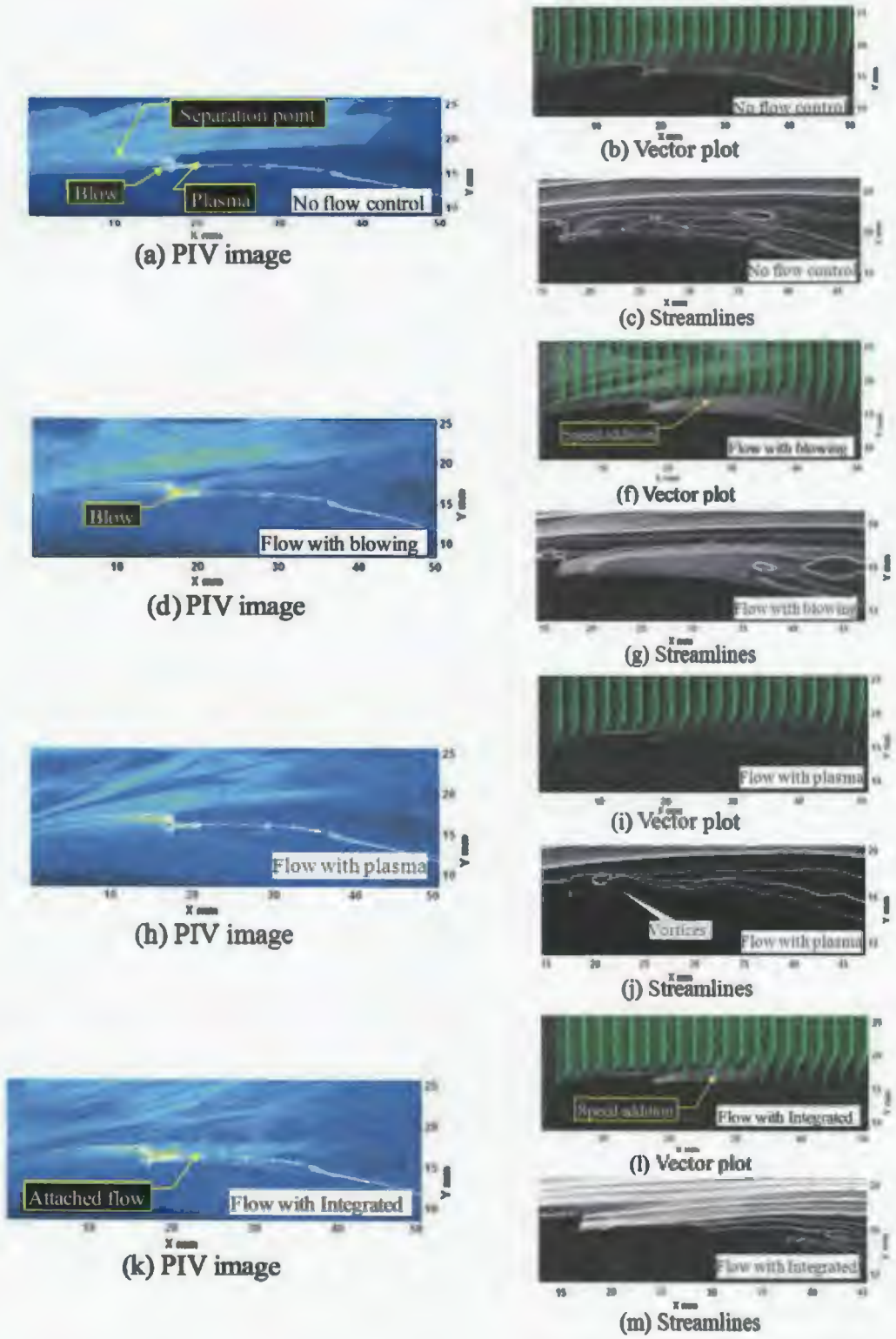

Figure 4.28. Summary of results for different flow control used for 3m/s freestream.

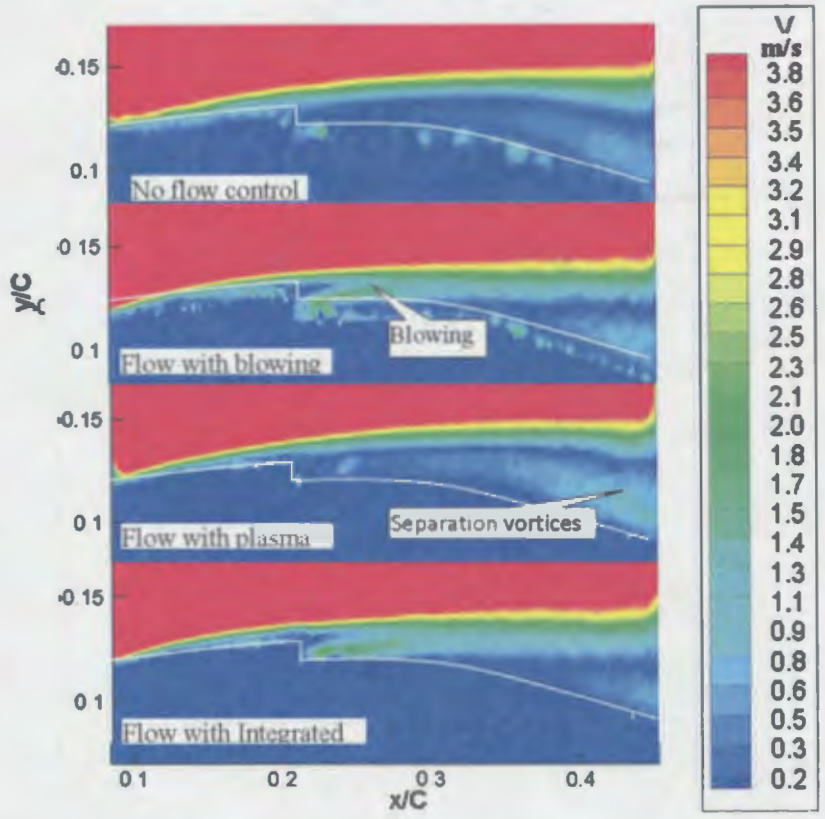

Figure 4.29.Speed contour plots for flow control methods investigated for 3m/s

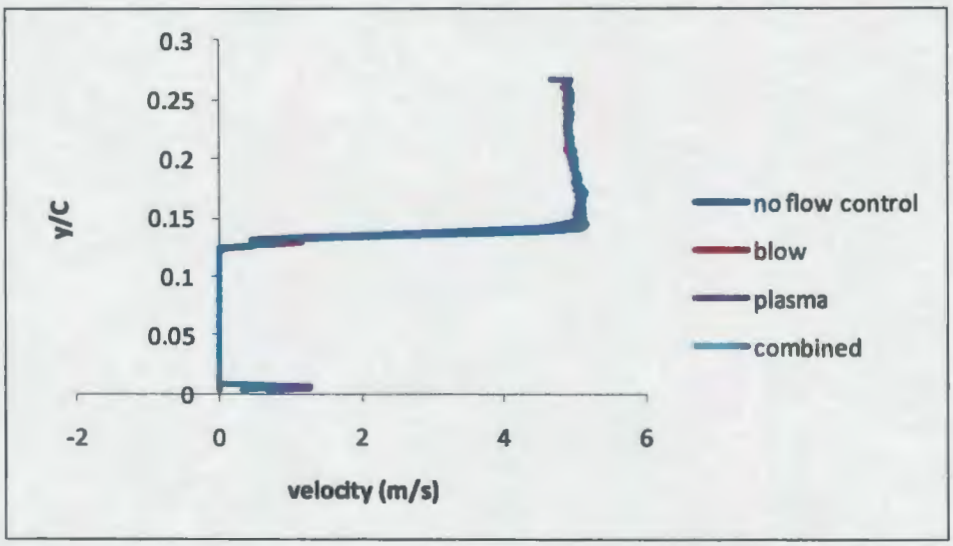

Figure 4.30. Velocity profile at 20% x/C of different flow control methods used at 3m/s

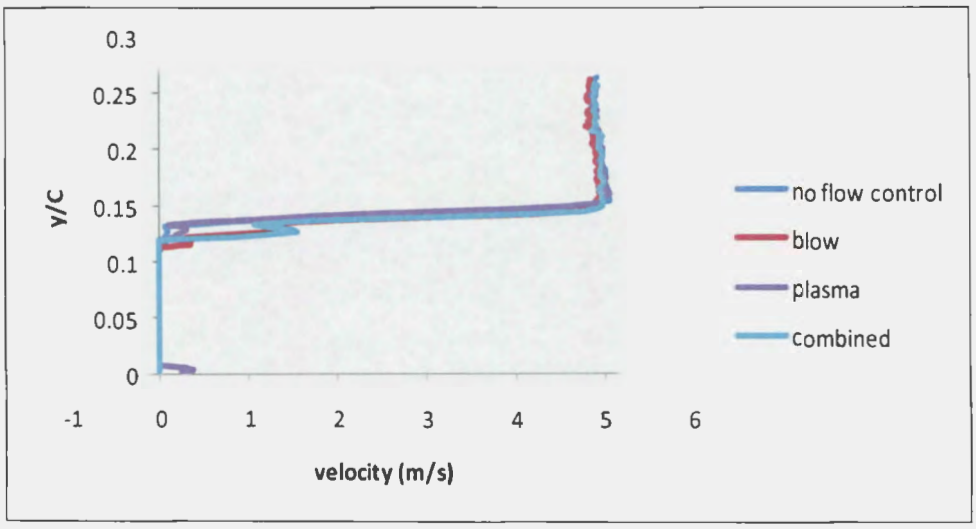

Figure 4.31. Velocity profile at 25% x/C of different flow control methods used at 3m/s

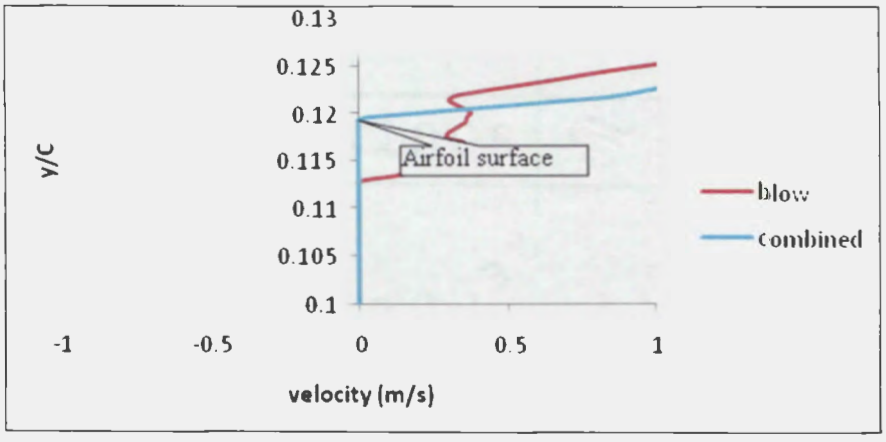

Figure 4.32. Magnified velocity profile at 25% x/C at 3m/s

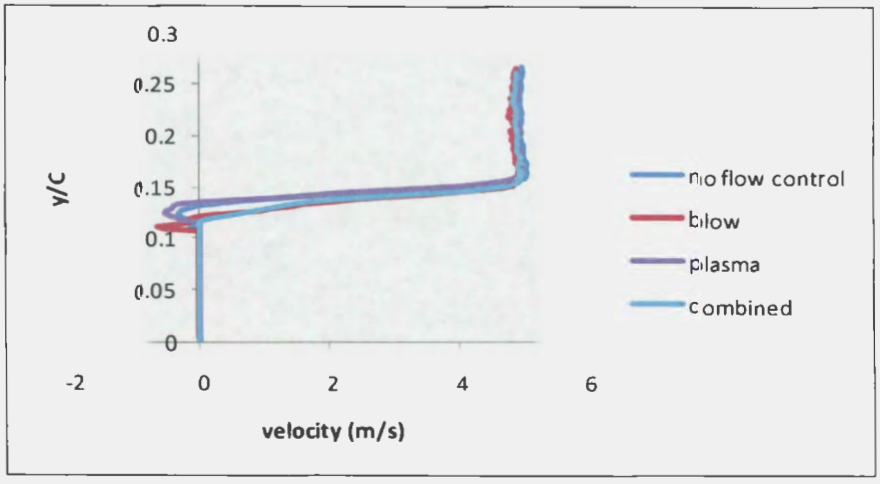

Figure 4.33. Velocity profile at 35% x/C of flow control methods used at 3m/s

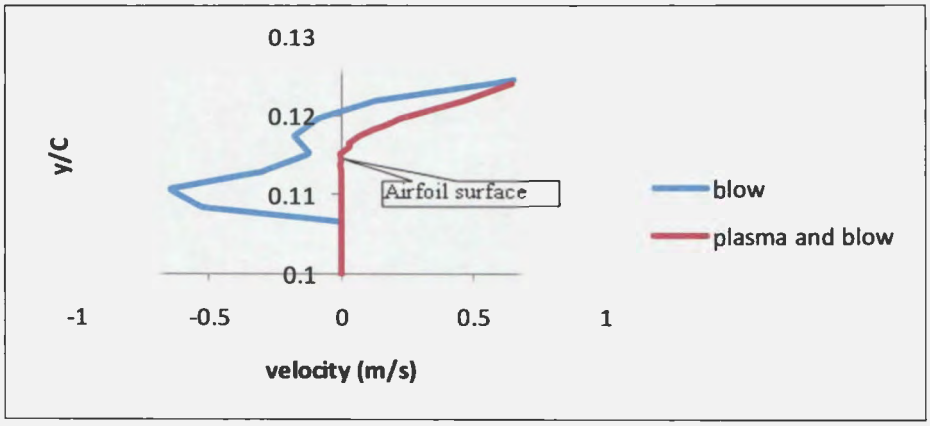

Figure 4.34. Magnified velocity profiles at 35% x/C for 3m/s

CHAPTER 5. CONCLUSION

The research aimed to develop a novel integrated flow control approach that can be used for flow separation control in low speed flows. Initially as a proof of concept, a vertically fired jet was incorporated with plasma actuators around the periphery and flow field investigations were performed to analyze the velocity incorporation due to plasma. The vertically fired jet initially without the plasma addition had peak velocity of 1.84 m/s in the center. However, when plasma was run along with the jet, the peak velocity was recorded 3.00 m/s. This significant improvement of velocity was possible due to the momentum incorporation by plasma. The total momentum addition from plasma was calculated as 1.951×10^{-4} (kg*m)/s which corresponds to 165.7 % increase in momentum and 63% reduction in blowing ratio, B.

Since the plasma integrated blowing was successful in velocity and momentum increment in a vertically fired jet, it proved to have great potential to also be effective in aerodynamic flow separation control. For analyzing the integrated effect in airfoil, NACA 0025 airfoil was investigated with the integrated plasma-blowing approach. Before incorporating the integrated control method on the airfoil, the separation location was determined using PIV techniques to find an optimum %x/C location on the airfoil so that separation can be effectively eliminated. The investigation predicted 25% x/C to be the most optimum place for incorporation of aerodynamic flow control.

Two different freestream velocities were investigated with integrated flow control i.e. 3m/s and 4.5 m/s. The airfoil was at 10 degree angle of attack. The integrated control was run with blowing of $C\mu = 0.0005$ and plasma at 2.4 KVolts rms,

frequency of 8KHz. In the experiments for 3m/s freestream, it was revealed that, the energy of single plasma or single blowing could barely make any influence in flow separation. However, when the integrated control was used, it was successful in minimizing the flow separation. When the velocity profiles were compared of different flow control method used at 35% x/C, 0.016 % y/C chordwise location, it was revealed that for the integrated control there was 110% increase in near wall velocity compared to the case where no flow control was used.

Future work: Although, the integrated control was successful in altering separation for 3m/s freestream, for 4.5 m/s freestream, was found to be producing inadequate amount of energy. This happened due to separation condition change over NACA airofoil when blowing slot was incorporated. Further experiments would be needed to better understand the integrated control performance in different speed and airfoil angle condition. A computer simulation model could also be effective not only to find optimum flow control parameters, but also to find proper location to place the integrated control. In this context, a preliminary computer model was built in ANSYS-CFX to perform two dimensional flow analyses. Figure 5.1, represents the mesh block of the model. For the study, a rectangular computational domain was generated that extends upto 10 times chord lengths in all directions and is composed of 112,000 cells. To the incorporate the blow/plasma affect a second two dimensional domain was generated consisting a total cell no of 160,000 having the same chord length. In case of angle of attack the same model is used but the freestream conditions were adjusted considering the angle of attack effects on them. The blowing effect was modeled using a tangentially contoured slot located at 25% x/C location. The opening for blowing was

kept as 2.54 mm (0.1 inch) covering the whole span. Similar computational approach was also performed by Tongchitpakdee[40] et al, Chang[41]et al and McGowan[42] et al.

To capture the effect of boundary layer a total of 35 inflated layer was created along the periphery of the airfoil. First layer thickness was chosen as y+ and y+ was set to 1.00. The solution was assumed to be in steady state and is not to be time accurate. The solver was chosen to be in high resolution and resolution value was chosen to be 300. Turbulence model was chosen as Shear Stress Transport with Gamma Theta model. In the rectangular flow regime inlet, outlet, top and bottom boundaries are set as opening. The blowing/plasma boundary was set as an inlet boundary. Side walls are set with symmetric boundary conditions. The airfoil boundary was set as no slip wall. The preliminary results can be seen in Figure 5.2.

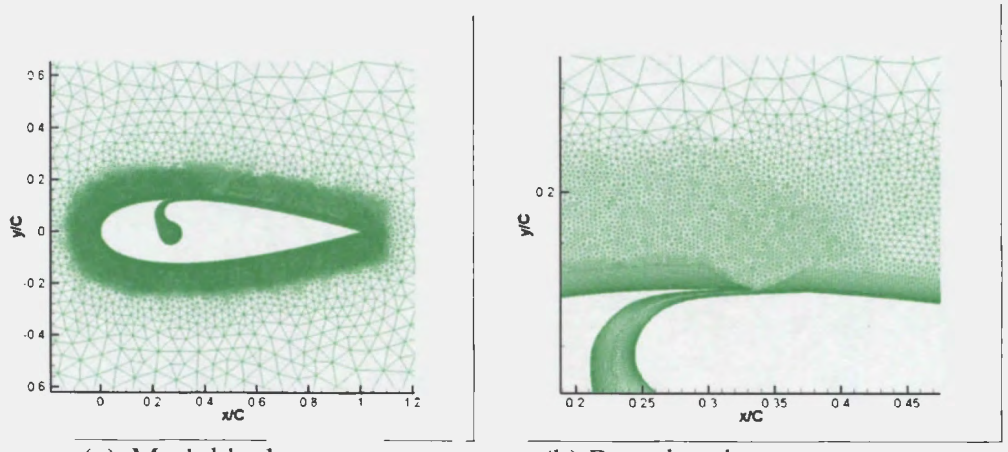

(a) Mesh block (b) Boundary layer

Figure 5.1. Mesh generated in ANSYS-CFX mesh

Although the results presented significant separation delaying due to the incorporation of flow control, the model would need major modifications in capturing boundary layer flow dynamics, which is a crucial part of any separation control

research. With the modification incorporated, the model would be more capable of predicting and capturing flow dynamics of the integrated control.

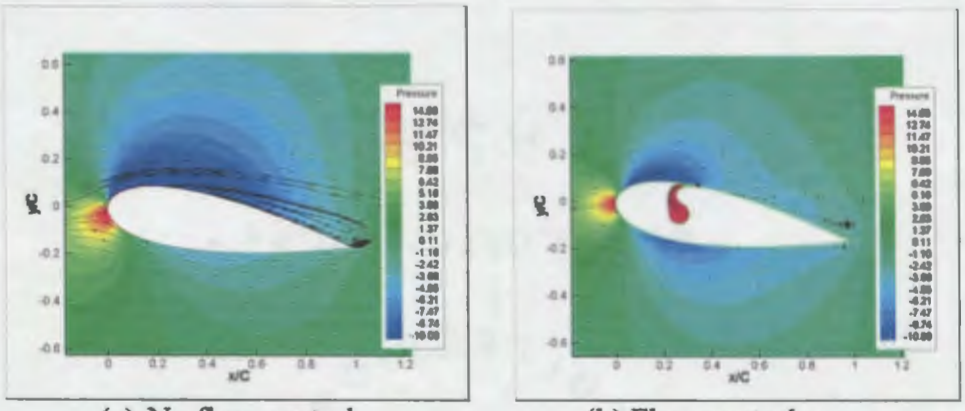

(a) No flow control (b) Flow control on

Figure 5.2. Streamlines in Pressure contour at 4.5 m/s, $\alpha = 10^{o}$

Accomplishments: Two posters were presented in the 2008 and 2010 ND EPSCoR State Conference based on the research findings. A conference paper has also been submitted in 2010 AIAA Conference. The paper decision is still pending.

APPENDIX: OTHER EXPERIMENTS

The integrated flow control research needed construction of a research facility to ensure quality. Apart from the experiments mentioned in chapter 3 and chapter 4, several other experiments were performed in the course of establishment of experimental facility. Calibrations and characterizations of different experimental equipments were also needed to be done. In this section, results are presented for necessary experiments that were performed for characterization of windtunnel, Airfoil Angle Setup, Determination of experiment domain, Blowing Characterization and Hotwire calibration.

A.1.Windtunnel Speed Characterization

Since the windtunnel used in the integrated flow control research was the first one to be used in any research work, speed characterization was performed to check stability and consistency of the tunnel. Speed measurement was performed using the Pitot static probe connected to the Omega differential pressure transducer and traversing mechanism. The frequency of data acquisition in the transducer was 10 kHz. Airfoil was not present in the test section in these set of experiments. The Pitot probe was placed manually in different spanwise horizontal positions and traversed in vertical direction for a particular velocity profile. The total horizontal traverse was 17 cm. Data was collected at 36 different locations across this 17 cm wide area each being 5 mm apart. For every single horizontal station, the pitot probe was traversed from the test section base to 250 mm upwards using Velmex VXM stepping motor traverse system. The speed contour for instantaneous velocity can been in Figure A.1. It is evident from the speed contour that there had been no major fluctuation of velocity in the test section.

The flow was found to be symmetric along the test section midspan. Velocity information was also obtained with hotwire probe and PIV system to check the consistency of reading among the equipment used. A slight inconsistency between the velocities recording equipments was found. Figure A.2 represents the illustration of the inconsistency. The velocity information obtained by the PIV was approximately 1 m/s higher than the velocity recorded by the pitot probe.

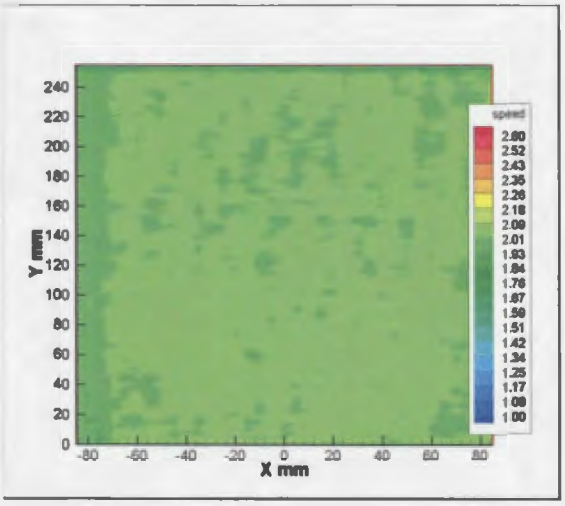

Figure A.1. Speed contour of wind tunnel test section

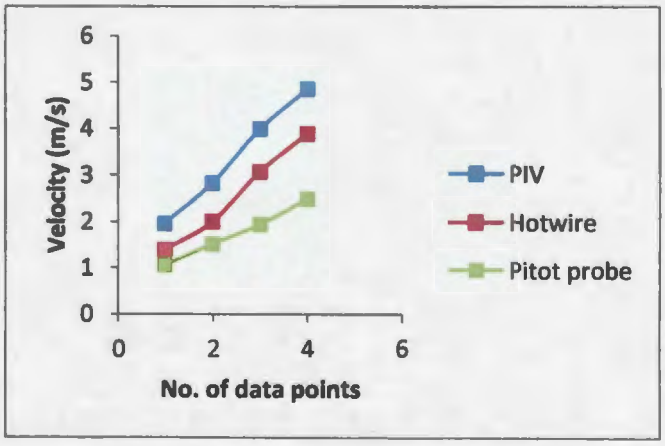

Figure A.2. Velocity comparison of equipment used

Data Repeatability: The pressure distribution data was checked for repeatability. In this particular case, the airfoil was set to 3m/s free stream velocity with zero degree angle of attack. Two sets of pressure data over the airfoil suction and pressure surface was collected with an interval of ten seconds. It was found that the data were reasonably consistent and maximum fluctuation was observed to be 3.5 %. Similar experiment was also performed for 4.5 m/s free stream and in this case maximum fluctuation was observed as 5.5%. Details can be found in Table A.1 and Table A.2.

Table A.1. Data repeatability results for 3m/s freestream

Location	x/C	ΔP Pa(run1)	ΔP Pa(run2)	%diff
Suction surface	0.11	-4.67505	-4.62555	1.058793
	0.208	-4.95089	-4.94054	0.209195
	0.30725	-3.99304	-4.01509	-0.55223
	0.4085	-3.2884	-3.26895	0.591533
	0.52493	-3.1326	-3.12277	0.313853
Pressure Surface	0.1579	-4.82177	-4.93362	-2.31968
	0.2574	-4.30125	-4.25154	1.155599
	0.3639	-3.45665	-3.4025	1.566386
	0.4582	-3.10431	-3.10379	0.016686

Table A.2. Data repeatability results for 4.5m/s freestream

Location	x/C	ΔP Pa(run1)	ΔP Pa(run2)	%diff
Suction surface	0.11	-11.6419	-11.8278	-1.59712
	0.208	-12.5575	-12.6422	-0.67445
	0.30725	-10.6747	-10.524	1.411514
	0.4085	-8.5835	-8.66695	-0.97229
	0.52493	-8.04331	-8.02773	0.193645
	0.6081	-7.91904	-7.89578	0.29364
	0.7081	-8.12662	-8.04769	0.97125
	0.808	-4.63011	-4.37224	5.569324
Pressure Surface	0.1579	-12.4846	-12.3942	0.723885
	0.2574	-11.3563	-11.0623	2.588644
	0.3639	-9.14055	-8.97777	1.780769
	0.4582	-7.82729	-7.84701	-0.25184
	0.5581	-7.7075	-7.55647	1.959504
	0.658	-7.82103	-7.69784	1.575133
	0.7581	-6.85965	-6.61212	3.608542
	0.857658	-3.00075	-2.98338	0.579069

A.2. Airfoil Angle of Attack

As mentioned in the chapter earlier, the airfoil was set to desired angle using the rack and pinion mechanism connected to the airfoil tail. However, to set the airfoil to a specific angle, a reference point was always necessary. In the current research, zero degree angle of the airfoil was considered to be the reference. As NACA 0025 was a symmetric airfoil, in zero degree angle of attack, it would produce an identical Cp distribution for both suction and pressure surfaces. In the current research, this Cp distribution was obtained adopting trial and error method. Figure A.3 represents three separate plots of Cp distributions which are considered for obtaining airfoil zero degree. It can be seen from the figure that, the pressure distribution was initially not identical. In Figure A.3 (a), the pressure side Cp was higher than suction side Cp distribution. As the motor step was increased, we can see that the Cp distribution slowly started to change its shape and in Figure A.3.(b), we can see that the Cp distribution closely became identical. Increasing motor step further had changed Cp distribution again and this time from Figure A.3. (c) we can see that the suction surface pressure was higher than pressure surface. Hence, Figure A.3. (b) was finally considered as zero degree angle Cp distribution for the airfoil as both suction and pressure side Cp distribution was found identical in this case. Once the zero degree angle was obtained, the airfoil was set to its maximum angle. The number of motor steps required to produce that angle was recorded. From this information, the angular movement of the airfoil for each motor step was determined. It was found that for each motor step, the airfoil travelled 0.45 degrees.

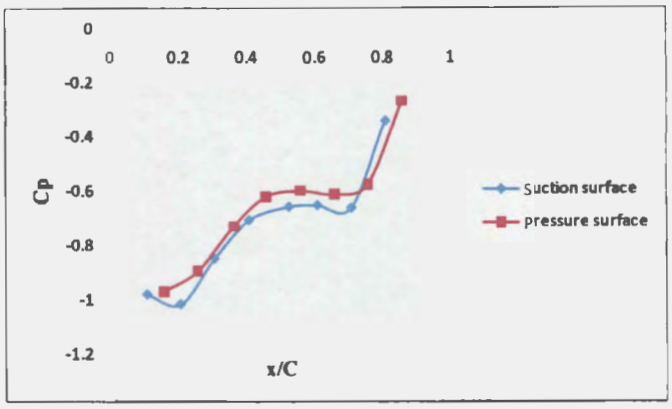

(a) 0.45 degree

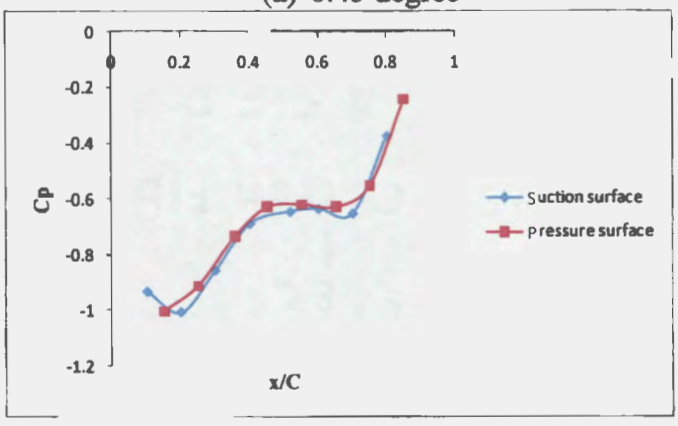

(b) Zero degree

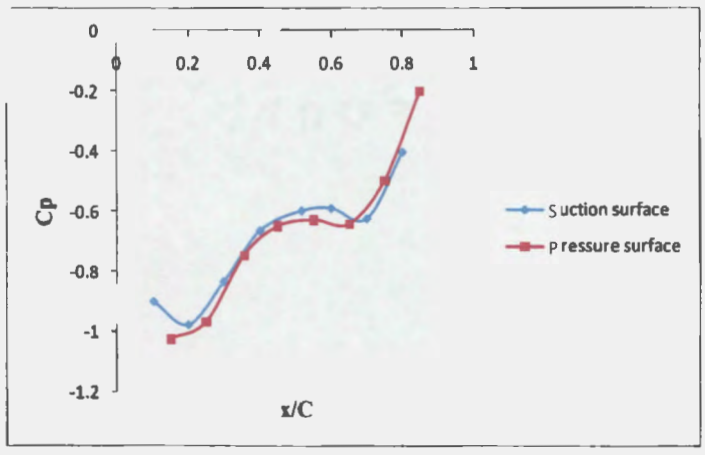

(c) -0.45 degree

Figure A.3. Airfoil zero degree angle Cp distribution determination

A.3. 2D Flow Field Determination

The current research was performed in two dimensional flow domain. Experiments were performed to determine the two dimensional flow field after the airfoil was placed in the tunnel test section. Speed contours and velocity profiles were obtained by traversing the pitot probe in horizontal and vertical locations. The horizontal traverse was 60 mm each side from the tunnel test section and vertical traverse was 200 mm upward from the test section base. Figure A.4 represents the speed contour plot obtained at 4.5 m/s with airfoil placed in windtunnel at zero degree angle of attack. In the plot, it can be seen that the placement of airfoil created a low speed region colored in green. When the airfoil was placed along with the plasma actuator on top of it, the appearance of speed contour was changed. In Figure A.4 (b), the influence of plasma actuator can be seen. The bubbles viewed in the speed contour was due to the placement of plasma actuator.

Since the plasma actuator was seen to incorporate disturbing effect on the flow domain, further experiments were performed to determine the region where the flow is free of these disturbances. It was found afterwards that in the center 2.54 cm wide region the flow is completely identical and creates an ideal 2D flow. Figure A.5 represents velocity profiles taken in the airfoil center, 1.3 cm left and right of the center of the airfoil. Figure also shows identical nature of the profiles.

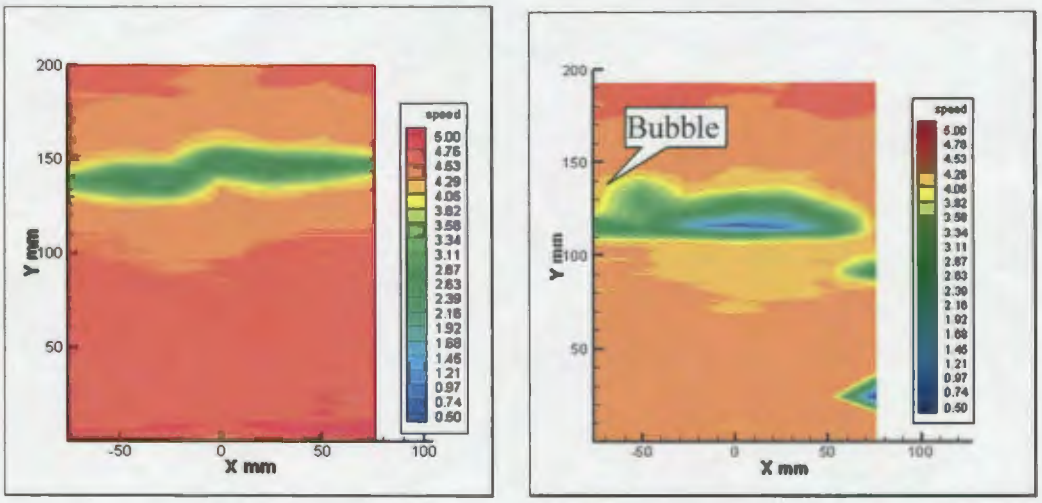

(a) (b)

Figure A.4. Speed contour of airfoil at 4.5 m/s and 10 degree angle of attack.

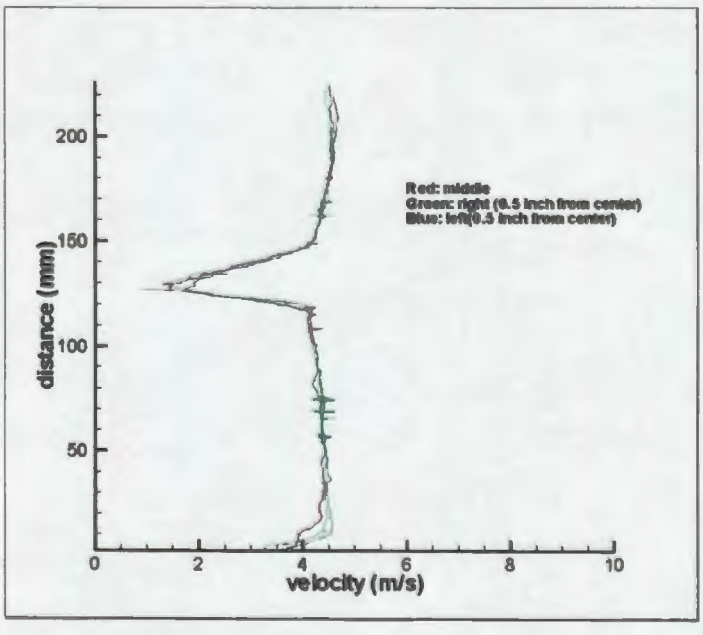

Figure A.5. Velocity profile of airfoil at 4.5 m/s and 10 degree angle

A.4. Blowing Experiments

Similar to the wintunnel flow field, an investigation was also performed for only blowing, to distinguish the 2D flow region. The pitot static probe was placed in three different horizontal locations along the blowing slot span. In each of the three locations, the pitot probe was traversed 12 mm vertically from the airfoil suction surface. Data was collected using the NI DAQ system with a frequency of 30 kHz. Figure A.6 shows the location and arrangement of the experimental setup. Initially a 2.54cm wide location in the midspan region of the blowing slot was investigation. However, the profiles were not identical along the 2.54 cm wide region. So the length has been reduced from 2.54 cm to 1.3 cm. Profiles were collected in three locations each 0.635 cm apart and displayed in Figure A.7. From the figure it can be seen that flow is two dimensional along that 1.3 cm wide region.

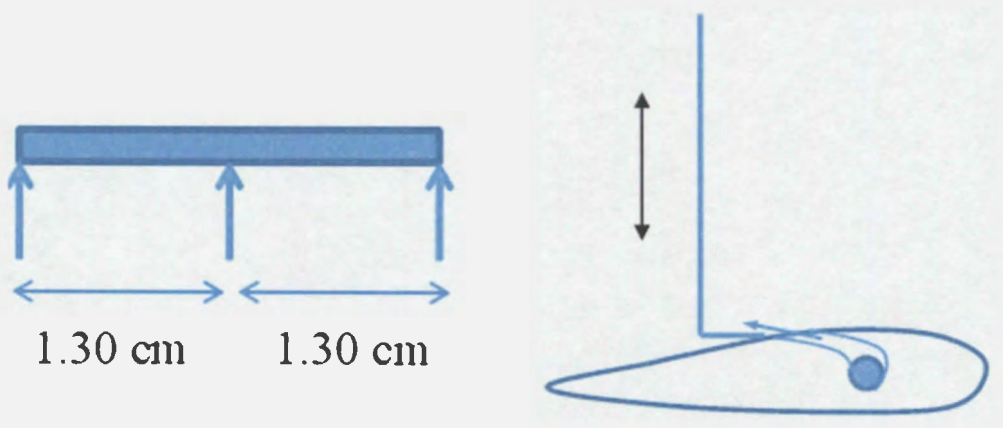

Figure A.6. Location and direction of blowing in Airfoil.

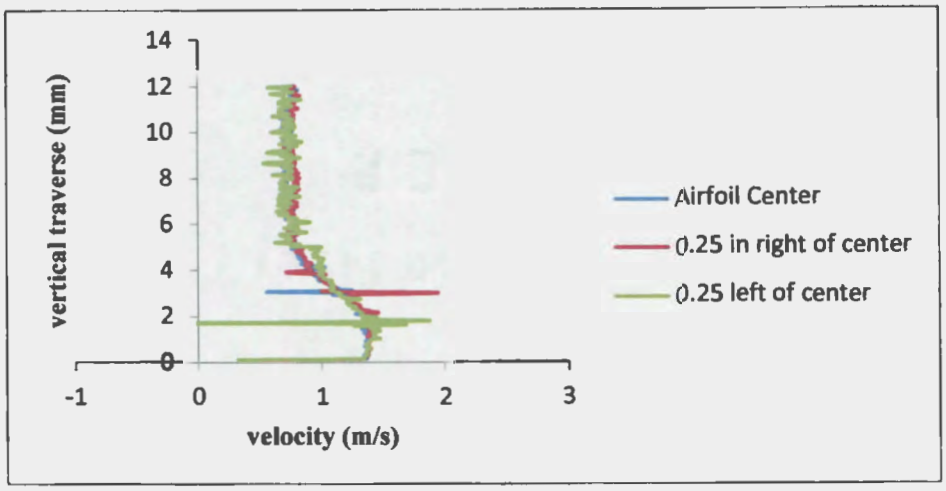

Figure A.7. Velocity profile of blowing in airfoil

A.5. Hotwire Calibration

The TSI IFA 300 hotwire sensor has been calibrated with an Air velocity calibrator (model TSI 1150) which is also manufactured by TSI Inc. The Air velocity calibrator is equipped with a differential pressure transducer with resolution of 0.05%. The hotwire sensor was mounted in the sensor holder of the Air velocity calibrator. 17 different flow velocities have been set with carefully controlling the coarse and fine adjusting valves of the calibrator. The details of calibration procedure can be found in the TSI IFA 300 manual. With obtained velocity information, a velocity vs. voltage relationship has been generated by the Thermal Pro software. The relationship is presented below where E is the bridge voltage: Velocity = 41.76598-109.79161 E +110.007939 E^2 – 51.32897 E^3 + 9.79293 E^4.

REFERENCES

[1] Corke, C., T., Enloe, C., L., Wilkingson, S., P., "Dielectric Barrier Discharge Plasma Actuators for Flow Control," Annual Review of Fluid Mechanics 2010. 42:505-29.

[2] Falkenstein, Z., and Coogan, J., "Microdischarge behavior in the silent discharge of nitrogen-oxygen and water-air mixtures," F. Phys. D 30:817-25 1997

[3] Roth, J. R. and Dai, X., "Optimization of the Aerodynamic Plasma Actuator as an Electrohydrodynamic (EHD) Electrical Device," AIAA Paper 2006–1203, 44th AIAA Aerospace Sciences Meeting and Exhibit, Reno, NV, Jan. 2006.

[4] Pons, J., Moreau, E., Touchard, G., "Asymmetric surface dielectric barrier discharge in air at atmospheric pressure: electrical properties and induced airflow characteristics". J. Phys. D: Appl . pHus. 38(2005) 3635-3642

[5] Forte, M., Moreau., E., Jolibois, J., Touchard, G., Cazalens, M., "Optimization of a Dielectric barrier discharge actuator by stationary and non-stationary measurements of the induced flow velocity – Application to airflow control," 3rd AIAA Flow Control Conference. 5-8 June 2006, San Fransisco , California

[6] VanDyken, R. D., McLaughlin, T. E., and Enloe, C. L., "Parametric Investigations of a Single Dielectric Barrier Plasma Actuator," AIAA Paper 2004–846, 42nd AIAA Aerospace Sciences Meeting and Exhibit, Reno, NV, Jan. 2004.

[7] Post, M. L., Corke C., T., "Separation Control Using Plasma Actuators - Stationary and Oscillating Airfoils," AIAA paper 2004-841, 42d AIAA Aerospace Sciences Meeting and Exhibit, 5-8 January 2004, Reno, NV.

[8] Ramakumar, K., Jacob, J. D., "Flow Control and Lift Enhancement Using Plasma Actuators," AIAA 2005-4635, 35th AIAA Fluid Dynamics Conference and Exhibit, 6-9 June 2005, Toronto, Ontario, Canada.

[9] C. L. Enloe, T. E. McLaughlin, R. D. VanDyken, K. D. Kachner, E. J. Jumper, and T. C. Corke, "Mechanisms and Responses of a Single Dielectric Barrier Discharge Plasma Actuator: Plasma Morphology," AIAA Journal, Vol.42, No. 3, pp. 589–594, March 2004.

[10] Porter, C. O., Baughn, J. W., McLaughlin, T. E., Enloe, C. L., and Font, G. I., "Temporal Force Measurements on an Aerodynamic Plasma Actuator," AIAA Paper 2006–104, 44th AIAA Aerospace Sciences Meeting and Exhibit, Reno, NV, Jan. 2006.

[11] C. L. Enloe, T. E. McLaughlin, R. D. VanDyken, K. D. Kachner, E. J. Jumper, T. C. Corke, M. Post, and O. Haddad, "Mechanisms and Responses of a Single Dielectric Barrier Discharge Plasma Actuator: Geometric Effects," AIAA Journal, Vol.42, No. 3, pp. 595–604, March 2004.

[12] Roth, J.R., Sherman, D.M., Wilkinson .S.P, "Boundary Layer Flow Control With A One Atmospheric Uniform Glow Discharge Surface Plasma," AIAA paper 1998-0328. 36 th Aerospace Sciences meeting and Exhibit, Reno, NV. January, 1998

[13] Jacob, J., Rivir, R., Carter, C., "Boundary layer flow control using AC discharge plasma actuators," 2nd AIAA Flow Control Conference. 28 June – 1 July 2004. Portland, Oregon.

[14] Porter, C., O., Baughn, J., W., McLaughlin, T., E., Enloe, C., L., Font, G., I., "Plasma Actuator Force Measurements," AIAA Journal. Vol. 45, No 7, July 2007

[15] Rivir, R., White, A., Carter, C., Ganguly, B., Jacob, J., Forelines, A., Crafton, J., "AC and pulsed Plasma flow control," *42nd AIAA Aerospace Sciences Meeting and Exhibit,* 5-8 January 2004, Reno, Nevada.

[16] S. Leonov, V. Bityurin, N. Savischenko, A. Yuriev, and V. Gromov, "Influence of Surface Electrical Discharge on Friction of Plate in Subsonic and Transonic Airfoil," *AIAA 39th Aerospace Sciences Meeting and Exhibit*, AIAA, Paper 2001-0640, 2001

[17] Balcer, B. E., Franke, M. E., and Rivir, R. B., "Effects of Plasma Induced Velocity on Boundary Layer Flow," AIAA Paper 2006–875, *44th AIAA Aerospace Sciences Meeting and Exhibit*, Reno, NV, Jan. 2006.

[18] Bejawada, N., G., Mahmud, Z., "Parametric Investigation of a Dielectric Barrier Discharge Plasma Actuator," Master's paper, North Dakota State University, March 2010.

[19] Post, M. L., Corke, T. C., "Separation Control Using Plasma Actuator- Stationary and Oscillating Airfoils." AIAA paper 2004-0841, *42nd Aerospace Sciences Meeting and Exhibit, Reno*, Nevada, January 2004.

[20] Corke, C. T., He, C., Patel, M. P., "Plasma Flaps and Slats: An Application of Weakly-ionized Plasma Actuators." *AIAA 2004-2127. 2nd AIAA Flow Control Conference,* Portland, Oregon. June 2004.

[21] Corke, T.,C., Jumper, E. J., Post, M. L., Orlov, D., Mclaughlin, T. E. "Application of Weakly-ionized Plasmas As Wing Flow-control Devices," AIAA paper 2002-0350.

[22] Huang, J., Corke, T. C., Thomas, F. O., "Plasma Actuators for Separation Control of Low Pressure Turbine Blades." *AIAA Journal*, volume 44. No. 1, January 2006.

[23] Post, M. L., Corke, T. C., "Separation Control on High Angle of Attack Airfoil Using Plasma Actuators." *AIAA journal volume 42*, No. 11, November 2004.

[24] Hultgren, L. Sl, Ashpin, D. E., "Demonstration of Separation Delay with Glow-discharge Plasma Actuator," AIAA paper 2003-1025. *41st Aerospace Sciences Meeting and Exhibit,*. Reno, Nevada. January 2003.

[25] Greenblatt, D,. Schiile, C., Y., paschereit, C., O., "Dielectric barrier discharge flow control at very low flight Reynolds numbers," *AIAA journal.* Vol 46, No. 6, June 2008

[26] Post, M. L., Greenwade, S. L., Yan, M. H., Corke, T. C., Patel, M. P., "Effects of an Aerodynamic Plasma Actuator on an HSNLF Airfoil," AIAA 2007-638. *45th AIAA Aerospace Sciences Meeting and Exhibit.* Reno, Nevada. 8-11 January 2007

[27] Goksel, B., Rechenberg, I., "Active flow control by surface smooth plasma actuators". , Notes on Numerical Fluid Mechanics and Multidisciplinary Design, 2006, Volume 92/2006, 273-280, DOI: 10.1007/978-3-540-33287-9_34

[28] Jolibois, J., Forte, M., Moreau, E.," Application of an AC barrier discharge actuator to control airflow separation above a NACA 0015 airfoil: Optimization of the actuation location along chord," *Journal of Electrostatics 66 (2008) 496-503*

[29] Santhanakrishnan, A. and Jacob, J. D., "On Plasma Synthetic Jet Actuators," AIAA Paper 2006–0317, *44th AIAA Aerospace Sciences Meeting and Exhibit,* Reno, NV, Jan. 2006.

[30] Bottelberghe, K., and Mahmud, Z., " Low-Pressure Effects on a Single DBD Plasma Actuator"; 48th AIAA Aerospace Sciences Meeting and Aerospace Exposition, 4 - 7 Jan 2010; Orlando World Center Marriott; Orlando, Florida

[31] Bayt, R., L., Ayon, A., A., Breuer, K., S., "A performance Evaluation of MEMS-based Micronozzles." AIAA 97-3169. 33 rd AIAA/ASME/SAE/ASEE joint propulsion conference and exhibit. July 7-9, 1997/Seattle, WA

[32] McAuliffe, B., R., Sjolander, S., A., "Active Flow Control Using Steady Blowing for a Low-Pressure Turbine Cascade," *Journal of Turbomachinery,* Vol. 126, pp 560-569. October 2004.

[33] Weaver, D., McAlister, K., W., Tso, J., "Supperssion of Dynamic Stall by Steady and Pulsed Upper-Surface Blowing", *Journal of Aircraft*, Vol. 41.

[34] Weaver, D., McAlister, K., W., Tso, J., "Control of VR-7 Dynamic Stall by Strong Steady Blowing." *Journal of Aircraft*, Vol. 41, No. 6, November-December 2004.

[35] Culley, D., E., Bright, M., M., Prahst, P., S., Starizisar, A., J., "Active Flow Separation Control of a Stator Vane Using Surface Injection in a Multistage Compressor Experiment," ASME paper GT2003-38863. *American Society of Mechanical Engineers and the International Gas Turbine Institute Turbo Expo,* June 16-19, 2003. Atlanta,GA.

[36] Wong, C., Kontis, K., "Flow Control by Spanwise Blowing on NACA 0012." AIAA paper 2006-3676.

[37] Seifert, A., and Pack, L., "Dynamics of Active Separation Control at High Reynolds Numbers," AIAA Paper No. 2000-0409, *38th Aerospace Sciences Meeting and Exhibit*, Reno, NV, 2000

[38] Carter, C., J., Guillot, S., A., Ng, W., F., Copenheaver, W., W., "Aerodynamic Performance of a High-Turning Compressor Stator with Flow Control, "AIAA Paper-2001-3973.

[39] McManus, K., Magill, J., " Separation Control in Incompressible and Compressible Flows using Pulsed Jets". AIAA Paper 96-1948.

[40] Tongchipakdee, C., Benjanirat, S., Sankar, L., N., "Numerical Studies of the Effects of Active and Passive Circulation Enhancement Concepts on Wind Turbine

Performance, " AIAA paper 2006-198, *44th AIAA Aerospace Sciences Meeting and Exhibit*, 9-12 January 2006. Reno, NV.

[41] Chang, P., A., Slomski, J., Marino, T., Ebert, M., P., "Numerical Simulation of Two and Three Dimensional Circulation Control Problem," AIAA paper 2005-80, *43rd AIAA Aerospace Sciences Meeting and Exhibit,* 10-13 January 2005. Reno, NV.

[42] McGowan, G., Aoplarathnam, A., "Computational Study of a Circulation Control Airfoil Using FLUENT." *AIAA journal*, 2005, pp 539-554.